How to dynamite an ion?

(Methods for ion activation)

Guillaume van der Rest
Institut de Chimie Physique
Université Paris-Saclay

Tandem mass spectrometry

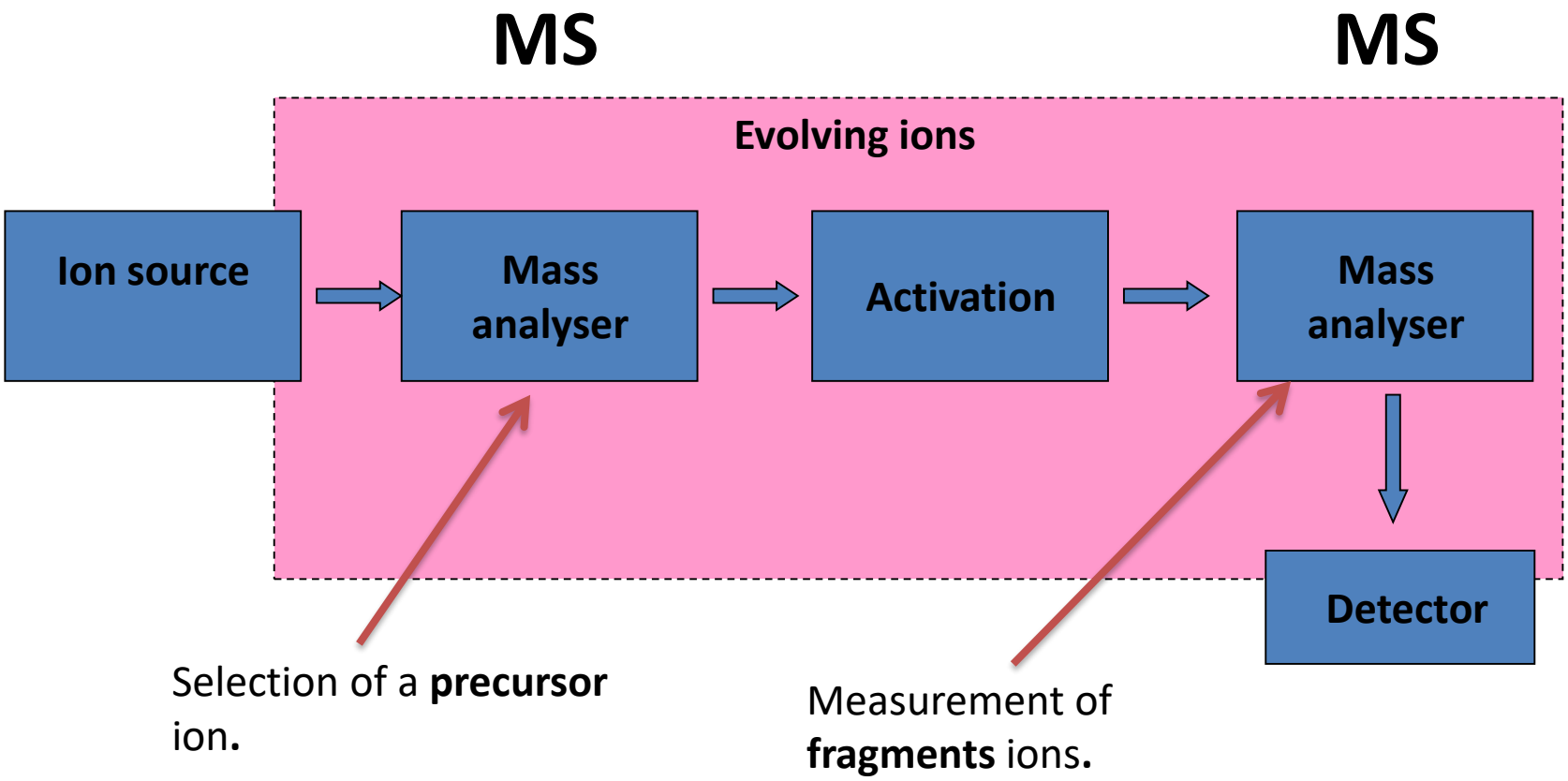

Ion activation in FT-ICR instruments

Collision cell = CID / ETD / Reactivity

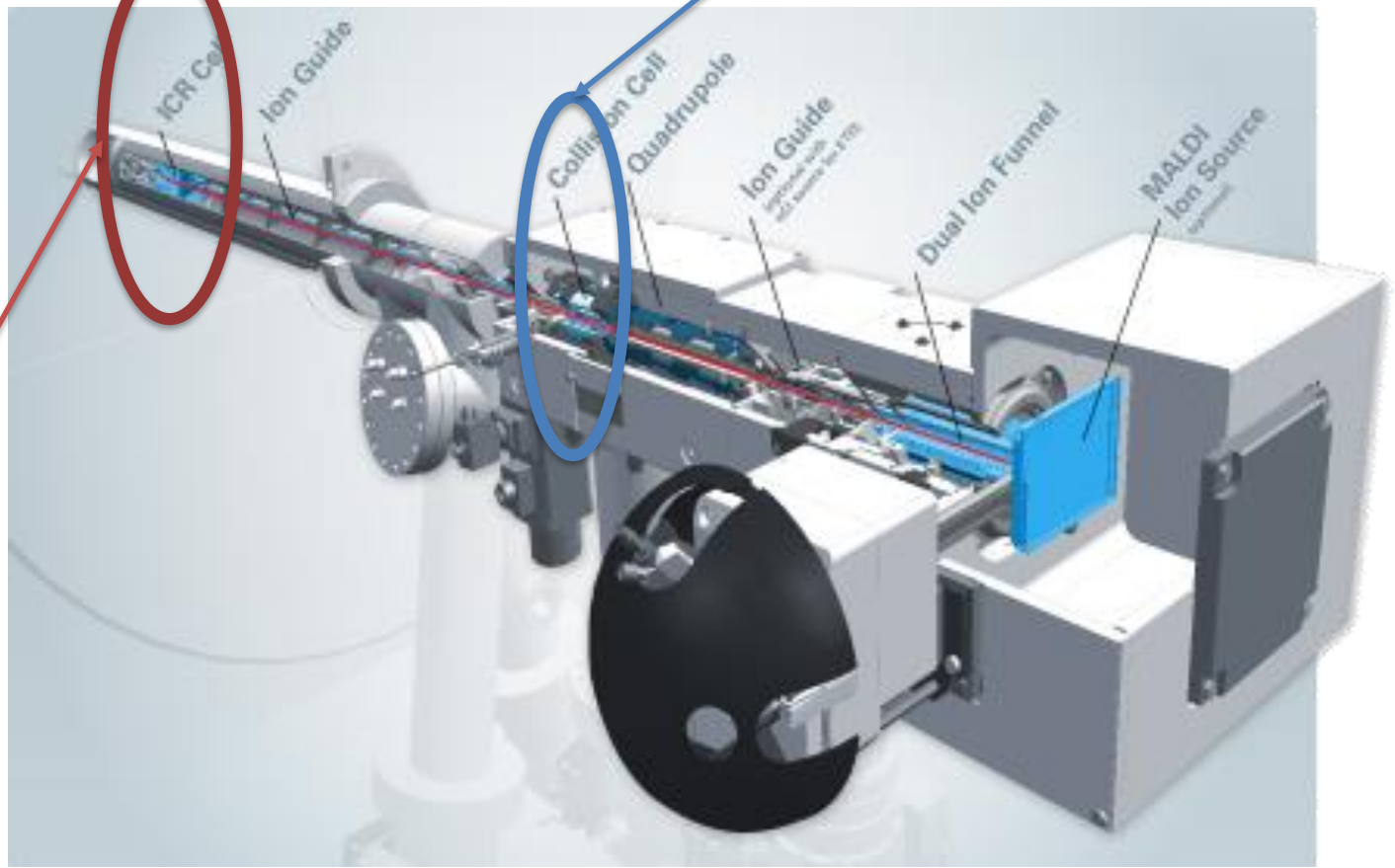

ICR Cell :
SORI – CID
ECD
IRMPD
UVPD
BIRD
…

Ion activation in Orbitrap instruments

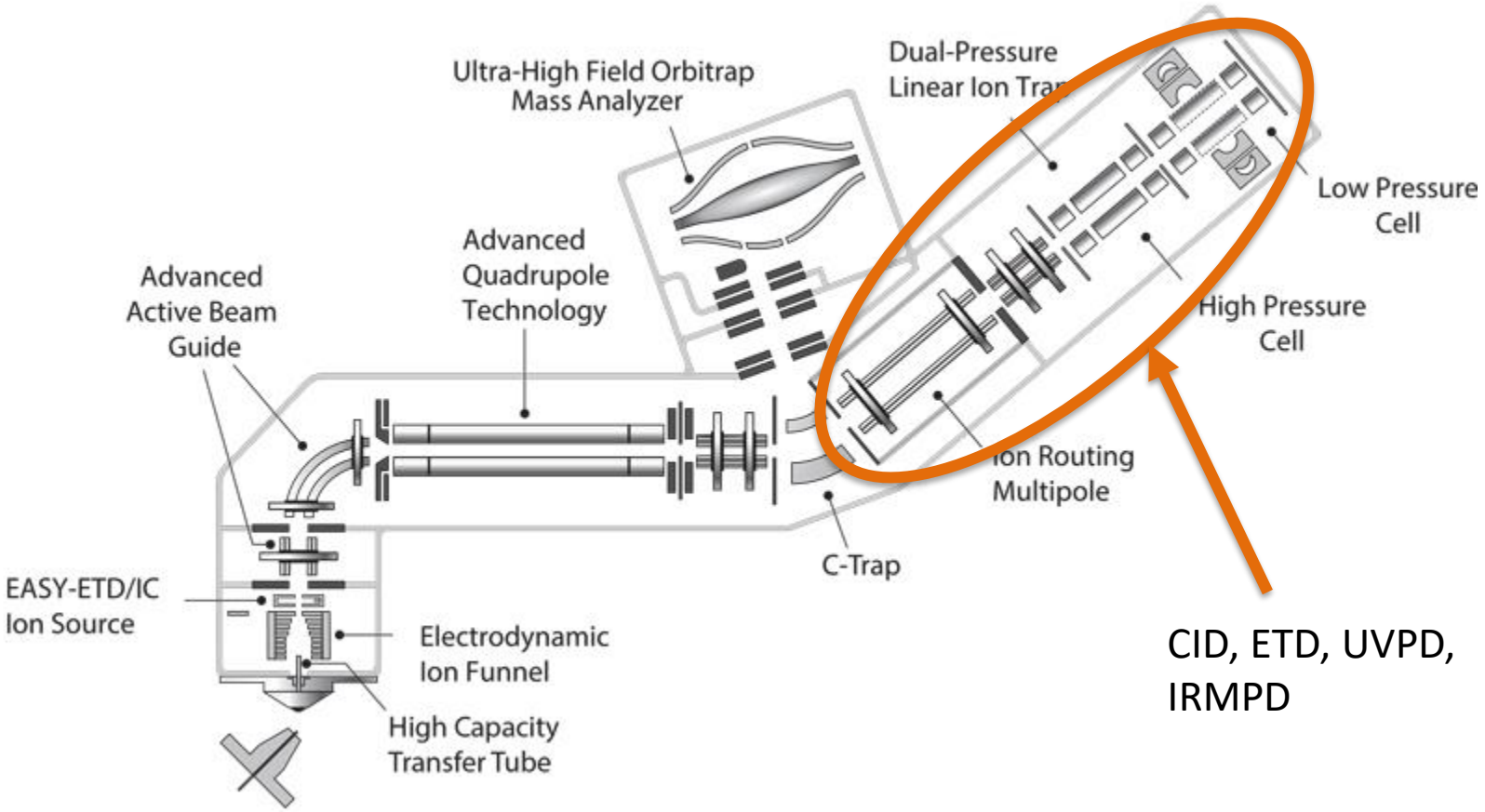

Kinetics and energetics of fragmentation

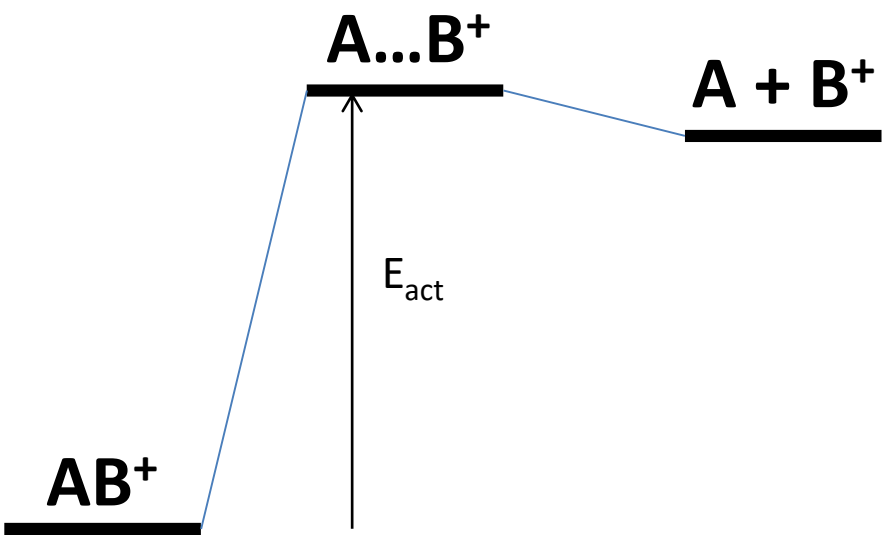

Fragmentation : generally an endothermic reaction.

Thermodynamics point of view :

$E_{int} < E_{act}$: No fragmentation

$E_{int} > E_{act}$: Fragmentation possible with a variable speed.

Kinetics point of view :
Unimolecular dissociation rate constant depends on the excess energy and transition state

Characteristic times can vary a lot depending on MS conditions.

Kinetic shift and the observation time window

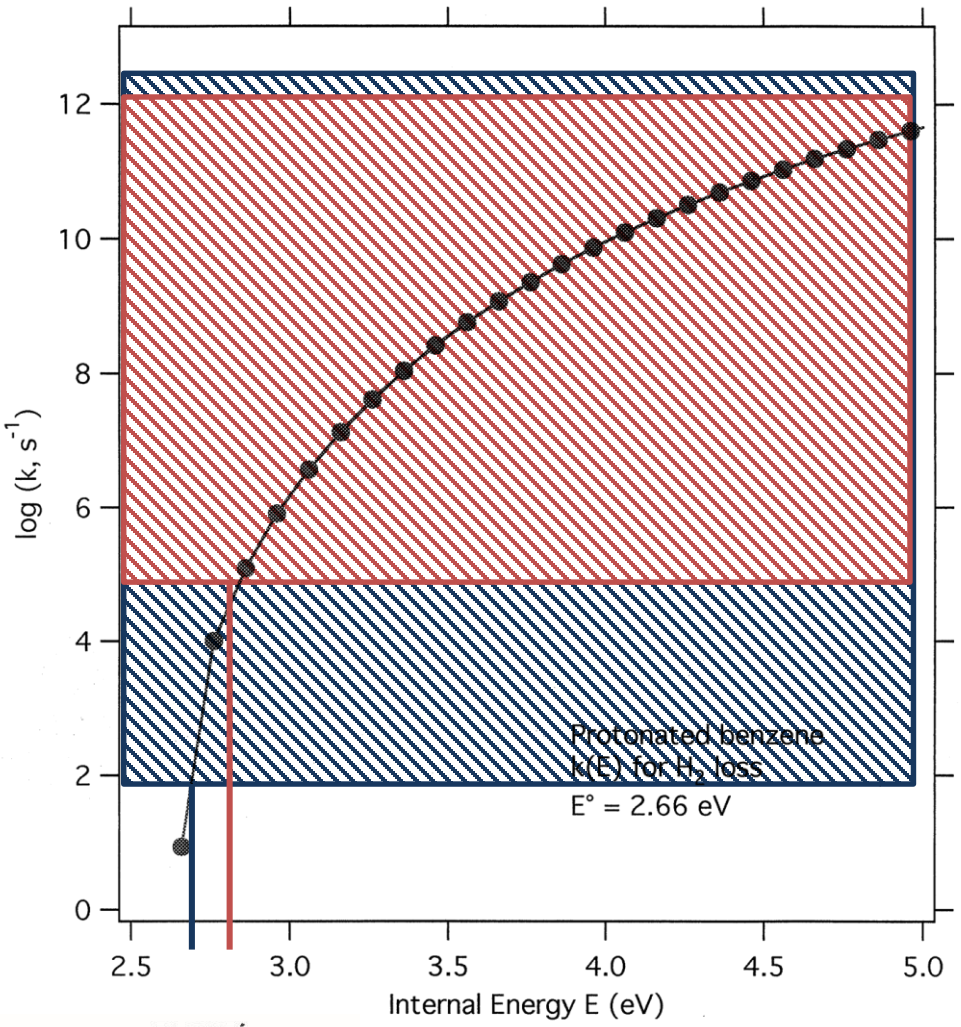

« Beam » type experiments.

« Ion trap » type experiments.

Precursor ion activation

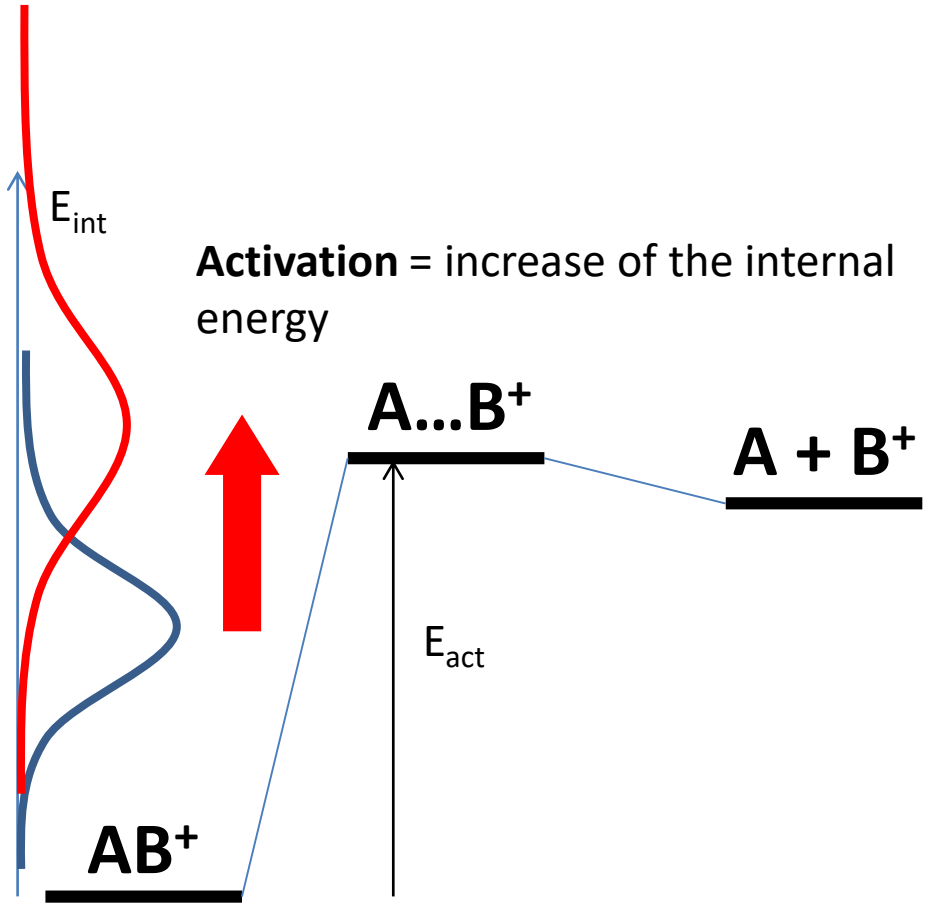

Activation methods:

Collision with an inert gas (CID)

Collision with a surface (SID)

Photon absorption :
UV (UVPD)
IR (IRMPD)

Reactive activations :

Reactive collisions with a gas
Cation / anion reaction
Interaction with electrons.

Collision induced dissociation

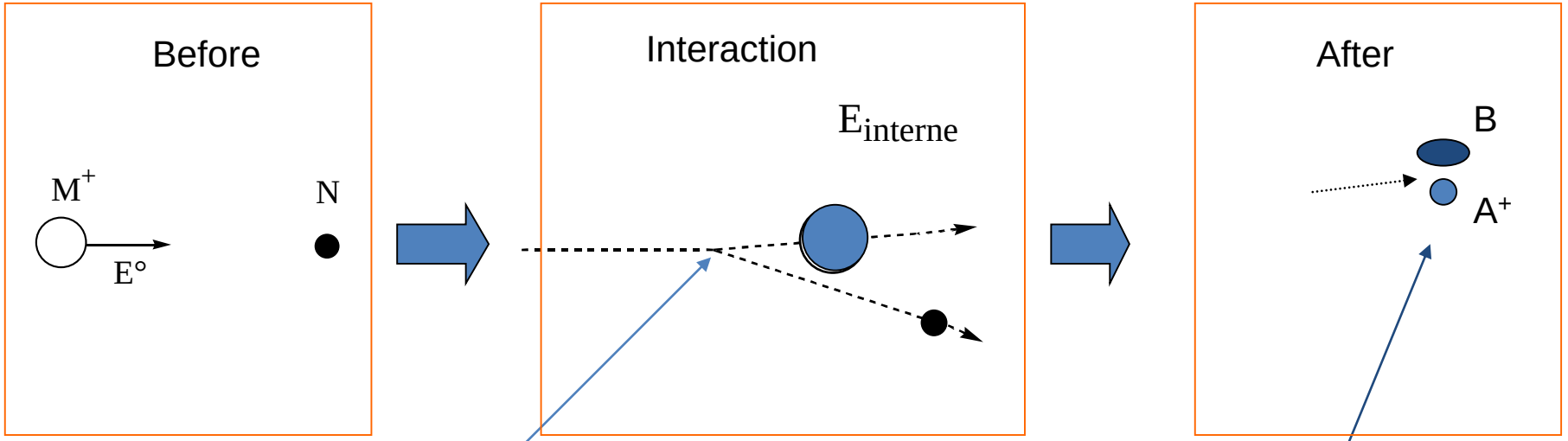

Collision: a fraction of the kinetic energy E°
Is converted into internal energy M^+

Activated M^+ ion fragments
at a given kinetics:
$M^+ \rightarrow A^+ + B$

Factors controlling the conversion into internal energy in the M^+ ion:

1°) Mass of M (the highest, the lowest conversion is possible in inelastic conditions),
2°) Mass of the neutral N (ex: 28 for N_2, 4 for He)
3°) Initial kinetic energy E°

Collision activation conditions

Classical gases in collision cells :

Ar, N_2, Xe, He

Control of the collision energy :

Acceleration of the ion before reaching activation region (HCD, Multipole cell)

rf excitation at secular frequency (ion trap)

The maximum amount of energy that can be transferred in a single collision is :

$$E_{int\ max} = [\ m(N)/(m(M) + m(N))\ ]\ E°$$

FT-ICR in cell collision activation

- Kinetic energy can be brought and controled through radiofrequency excitation :
  - Azimutal dipolar: resonant or non-resonant (SORI)
  - Axial dipolar: allows higher kinetic energies but with increased trapping potentials.
- Azimutal excitation is limited by the cell radius, and should take into account that ion excitation / detection is performed after:
  - Numeric application :
    - 7T, r = 3 cm, m/z 1000 (1+). Excitation at r_{max} : 2125 eV. Excitation at 10% r_{max} : 21,2 eV
- Presence of gas in the cell:
  - Pulsed injection of gas at pressures in the 10^{-5} - 10^{-7} mbar range
  - Pumping delays increase the overall experimental time

Resonant excitation

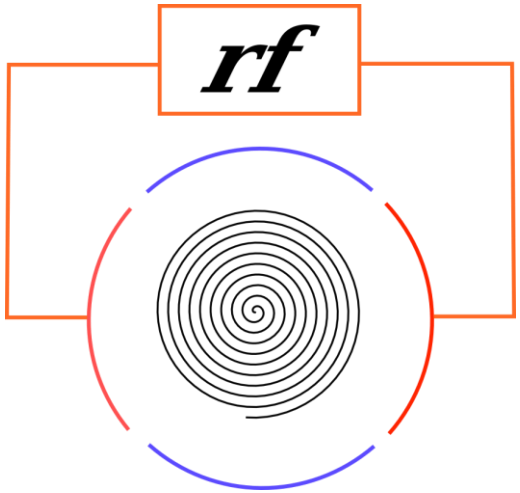

$$r = \frac{\beta_{dipolar} V_{\text{p-p}} t_{exc}}{2 d B_0}$$

$$E_{kin} = \frac{\beta_{dipolar}^2 q^2 V_{\text{p-p}}^2 t_{exc}^2}{d^2 m}$$

- Low energy available.

- Tight control of the energy in the single collision regime:
  - ➔ If the collision delay is calculated so as to have at most one collision during the delay, it is possible to know precisely the maximal energy that has been input in the ion, and to do truly energy-resolved CID.

Measuring fragmentaion activation energies

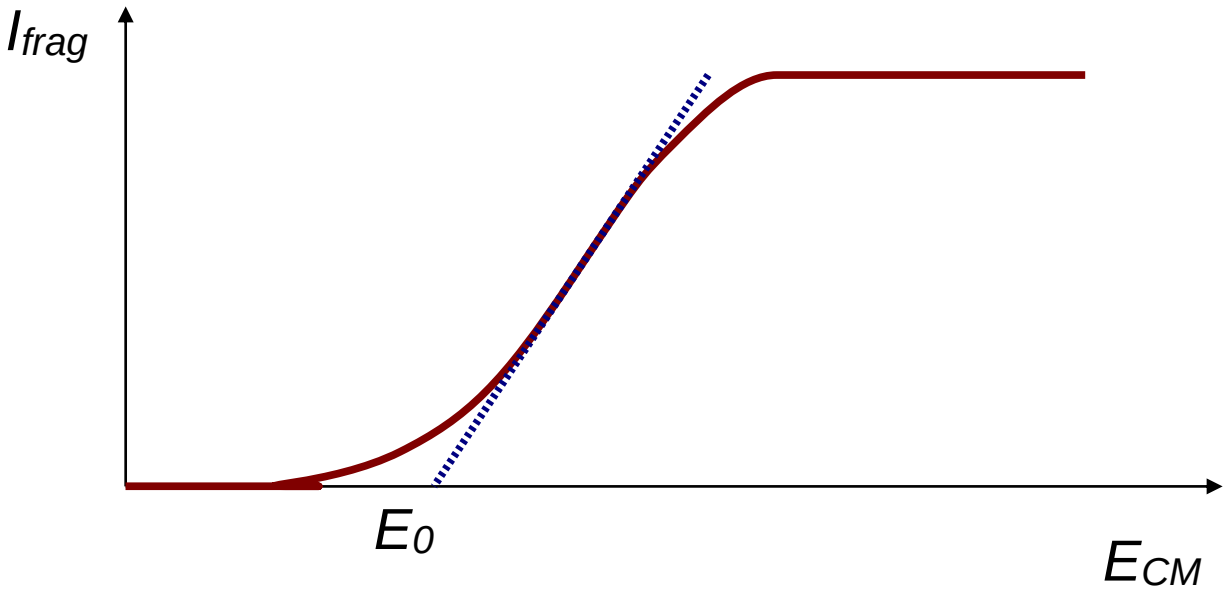

Since the collision model is simple, and the energy can be controlled by V_{p-p} or t_{exc}, E_0 can be extracted from the curve.
This gives access to experimental activation energies and bond dissociation energies.

Non-resonant : SORI

- SORI = Sustained Off-Resonance Irradiation

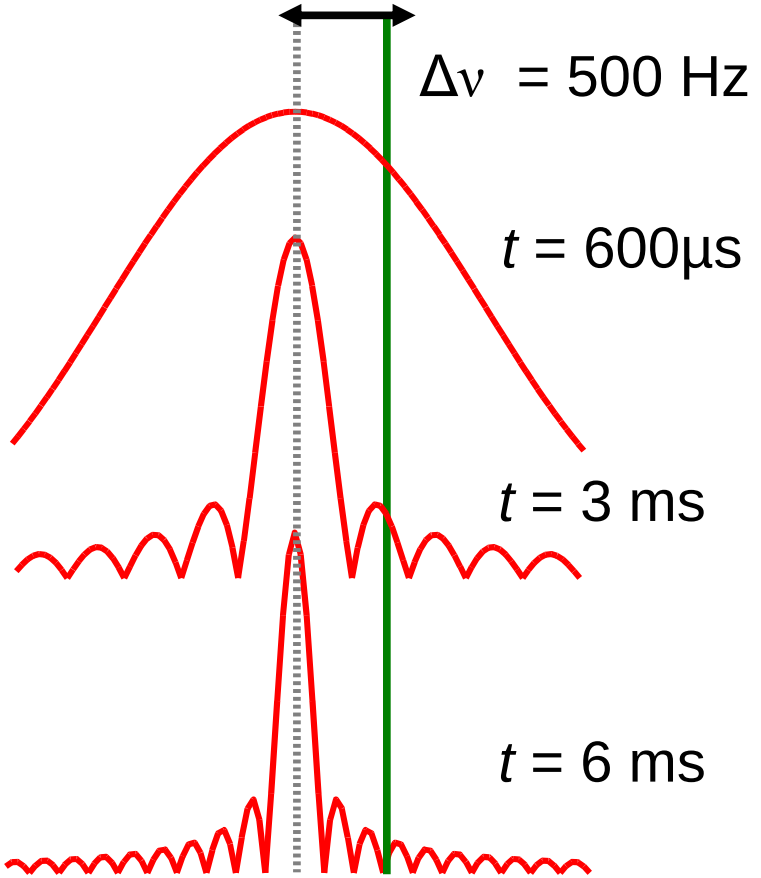

$$E_{kin}(\Delta\nu, t_{exc}) = \frac{\beta_{dipolar}^2 q^2 V_{p-p}^2 t_{exc}^2}{8d^2 m}\left(\frac{sin(\pi\Delta\nu t_{exc})}{\pi\Delta\nu t_{exc}}\right)^2$$

$$= \frac{\beta_{dipolar}^2 q^2 V_{p-p}^2}{8d^2 m(\pi\Delta\nu)^2}\left(sin(\pi\Delta\nu t_{exc})\right)^2$$

$$r(\Delta\nu, t_{exc}) = \frac{\beta_{dipolar} V_{p-p}}{2dB_0}\frac{sin(\pi\Delta\nu t_{exc})}{\pi\Delta\nu}$$

Ion movement in SORI-CID

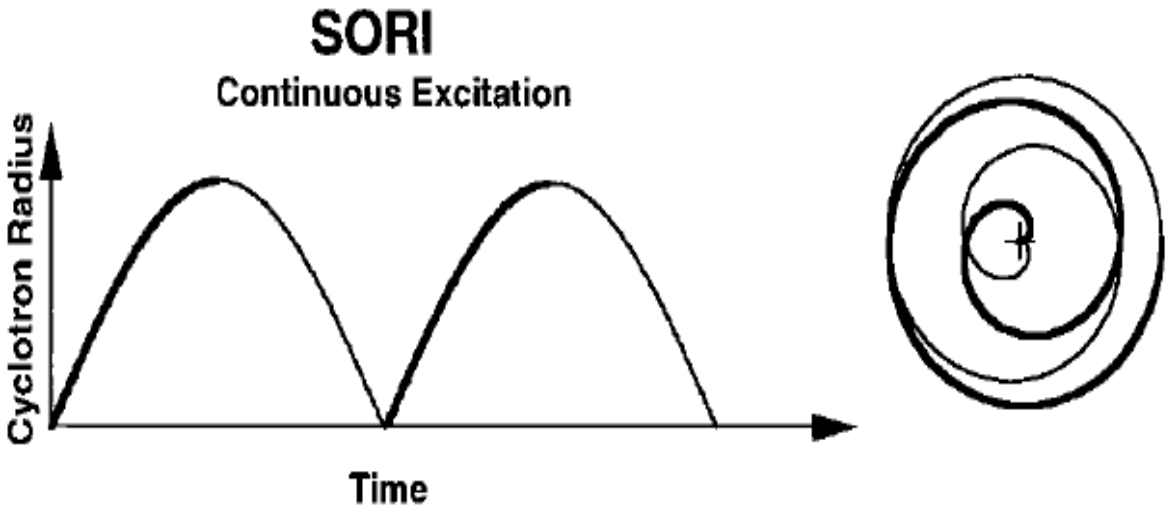

- Ions remain confined in a specific part of the cell.
- Excitation can last for long time (multiple collisions possible), as long as the precursor ion does not fragment.

$$\langle E_{kin}(\Delta\nu)\rangle = \frac{1}{2}\frac{q^2 V_{\text{p-p}}^2}{8d^2 m(\pi\Delta\nu)^2}$$

$V_{p\text{-}p}$ 10 V, 500 Hz offset, 6 cm diameter cell: 68 eV.
E_{max} : 135 eV
r_{max} : 7,6 mm (25% of cell radius)

WHY USE FT-ICR FOR ION PHOTODISSOCIATION ?

Ion storage in ICR cells

Dates back to before FT was introduced.

Photodissociation of the CH_3Cl^+ and N_2O^+ Cations

Robert C. Dunbar*

Contribution from the Department of Chemistry, Stanford University, Stanford, California 94305. *Received October 2, 1970*

Abstract: The ion cyclotron resonance technique was used to observe the photodissociation of the cations CH_3Cl^+ and N_2O^+ in the gas phase. Ions were trapped in the icr cell for periods of the order of seconds, which permitted the photodissociation process to be observed with wavelength-selected light. A cyclotron resonance ejection technique was employed to show that CH_3Cl^+ ions were being dissociated rather than the CH_3ClH^+ ions which were also present. The photodissociation cross section for N_2O^+ was found to be roughly 0.25×10^{-18} cm² without strong wavelength dependence between 4000 and 6500 Å. The cross section for CH_3Cl^+ showed a large peak at 3150 Å, having a value at that wavelength of 7.8×10^{-18} cm². Possible assignments of this peak are considered, and it is suggested that photodissociation occurs through an ion excitation involving a change in occupation of the bonding or antibonding orbitals of the C–Cl bond.

R.C. Dunbar, J. Am. Chem. Soc. **93**, 4354 (1971)

Ion storage in ICR cells

At low field, FT-ICR allowed **long storage times** for the ions.

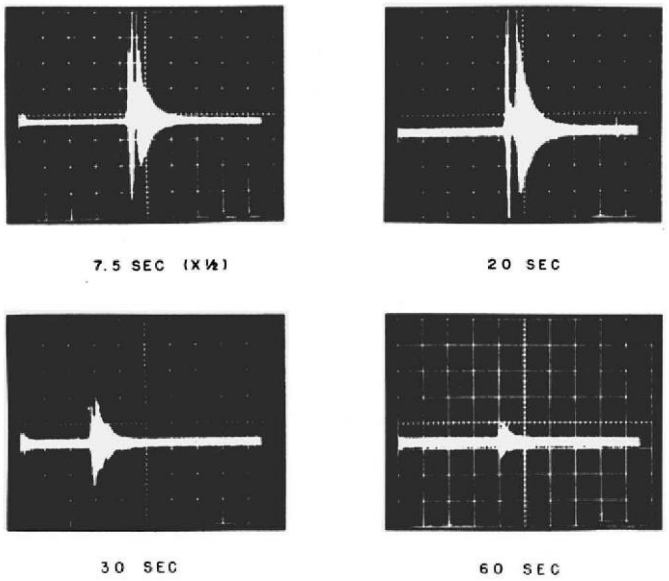

Figure 2. Ion trapping. The trapping of H_3O^+ ions under conditions of extremely long trapping is shown. The traces shown indicate a trapping time of about 30 sec for H_3O^+.

Wavelength tunability allows recording of an **action spectrum** of the CH_3Cl^+ ion.

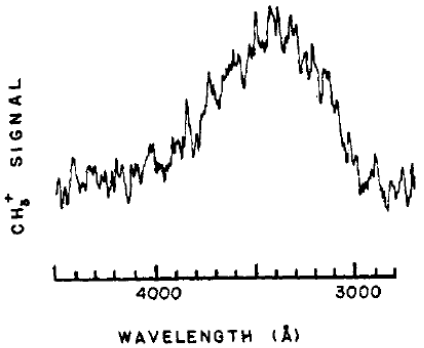

Figure 1. Production of CH_3^+ by photodissociation of CH_3Cl^+. The concentration of CH_3^+ in the icr cell is continuously monitored while the wavelength of the irradiating light from the monochromator is swept. The wavelength resolution (FWHM of the irradiating light) is 140 Å.

Ion beam and irradiation overlap

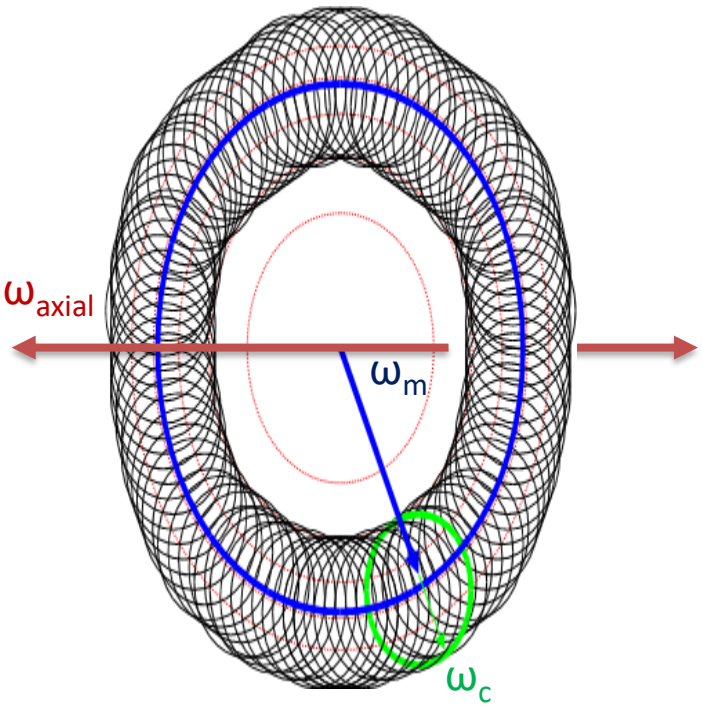

- Radiation needs to intersect the ion trajectory both in space and in time.
- Irradiation along the cell axis is the most usual setup.

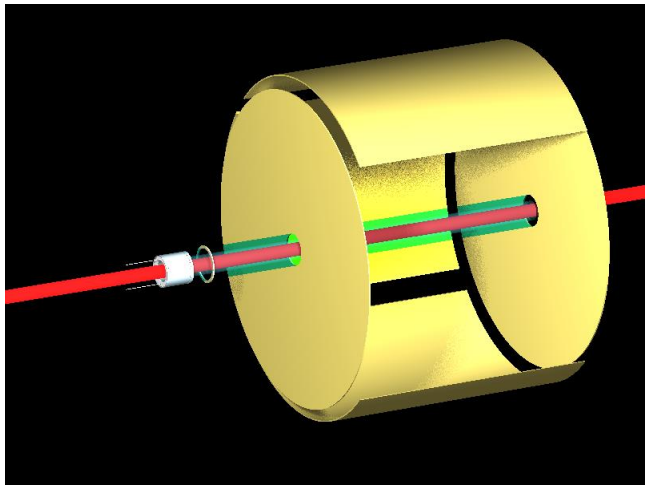

Ion beam and irradiation overlap

- On permanent magnet based instrument, irradiation can also be performed orthogonaly to the magnetic field.

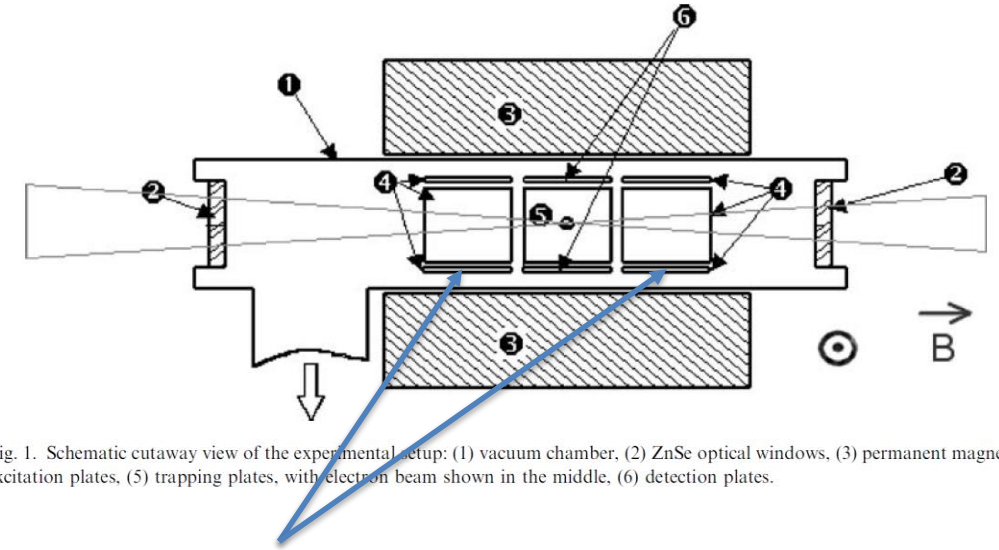

Fig. 1. Schematic cutaway view of the experimental setup: (1) vacuum chamber, (2) ZnSe optical windows, (3) permanent magnet, (4) excitation plates, (5) trapping plates, with electron beam shown in the middle, (6) detection plates.

Open ended excitation electrodes

*P. Maître et al. Nucl. Instrum. and Meth. Phys. Res. A **507** 541 (2003)*

Ion beam and irradiation overlap

- Issues with overlapping beams :
  - Highest power densities are achieved with tightly focused pulsed photon sources
  - FT-ICR is not optimal for this :
    - Axial motion is generally on the order of centimeters : requires very good on axis alignement of the light beam in order to cover the complete cloud.
    - Radial (magnetron / cyclotron) motions radius depends on the magnetic field, initial ion velocities but also alignment and centering of the cell axis and ion injection path. Order of magnitude: millimiter.
    - 3D ion traps perform much better (overall volume on the order of 1 mm^3)
  - Solutions :
    - Higher irradiation power with an unfocused beam (use of beam expanders in IRMPD for instance)
    - **(Pseudo) Continuous irradiation** : increase the irradiation time to average over ion positions (but beware that some ions might remain out of the beam).
    - **Pulsed irradiation :** timing and delay effects might dramatically change the results with a focused beam as the ion cloud sample will change over time.

Action spectrscopy vs absorption spectroscopy

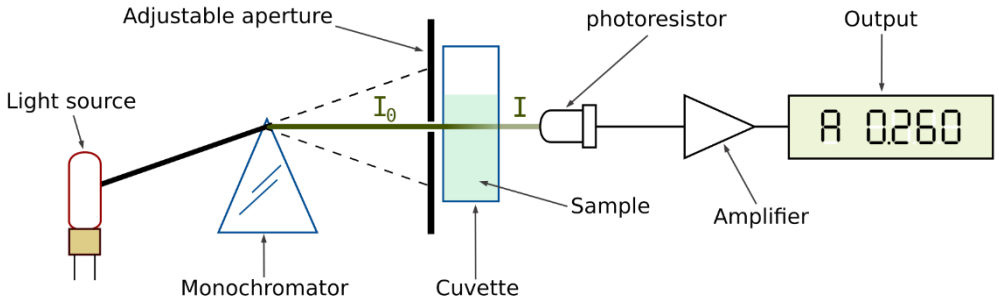

Standard spectrophotometer setup (source wikipedia)

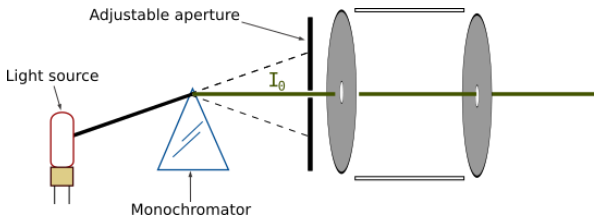

$$Eff = \frac{I_{frag}}{I_{prec} + I_{frag}}$$

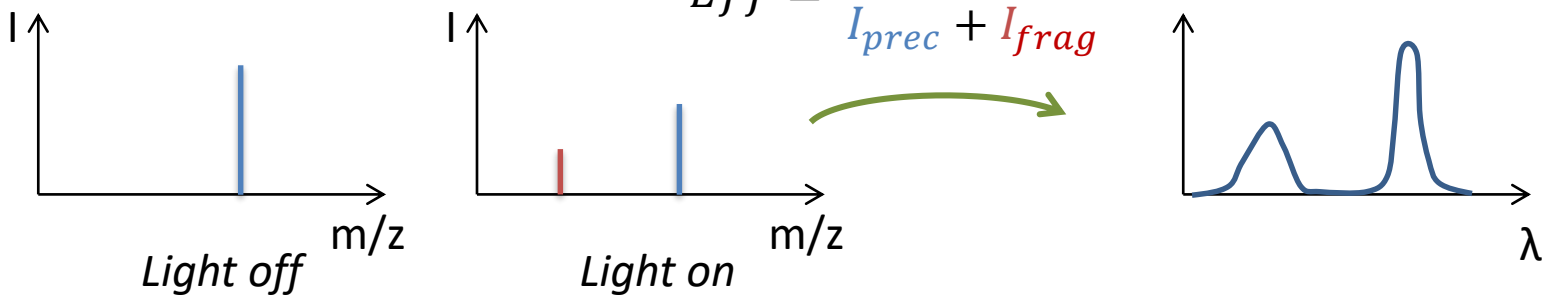

Pros and cons of FT-ICR vs ion traps for spectroscopy

- Cons :
  - Ion cloud overlap is more difficult to achieve compared to a 3D ion trap.
- Pros :
  - High resolution which can be achieved in the detection of product ions
  - Low pressure of the gas background : reduced thermalization effects.
    - Action spectroscopy assumes that absorption of a photon is related to fragmentation efficiency.

$$\text{Precursor} \underset{k_{-1}}{\overset{k_1(\lambda,I)}{\rightleftharpoons}} [\text{Precursor}]^* \xrightarrow{k_{uni}(E)} \text{Fragment}$$

k_{-1} is composed of a collisional and a radiative component. Minimization of the collisional component improves the result.
This is even more the case for multiple photon processes.

SINGLE PHOTON PROCESSES

Photon activation (UV – Visible)

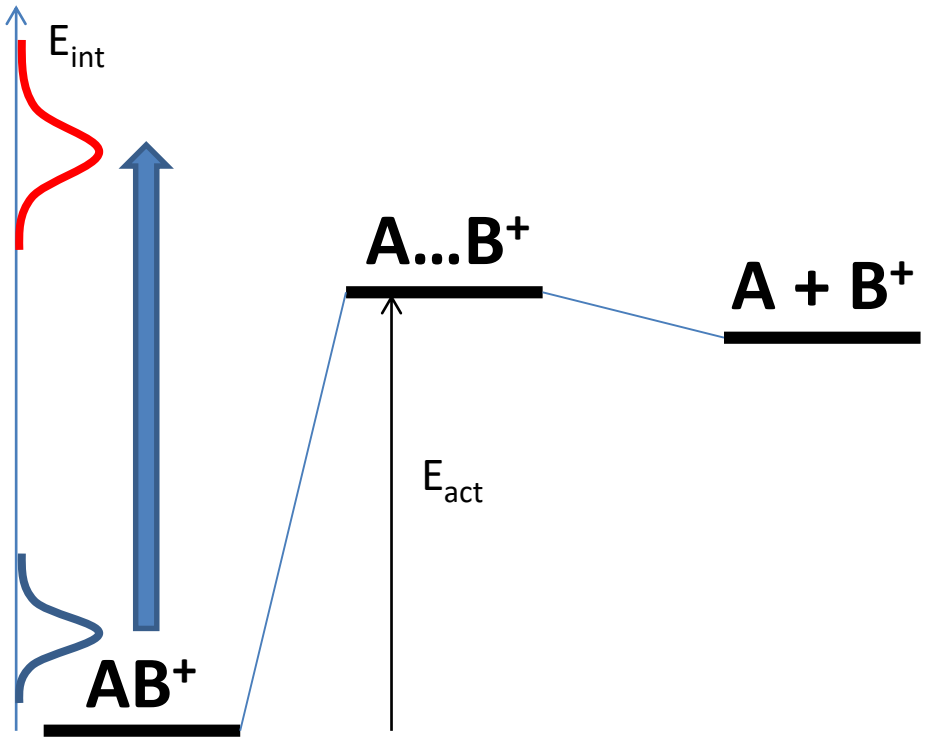

Single photon activation :

- Requires a photon with sufficient energy : ~ eV
- Requires an absorption band

- Proceeds through an electronic excited state, which can either directly dissociate or redistribute energy through intersystem crossing.

Lamp + monochromator

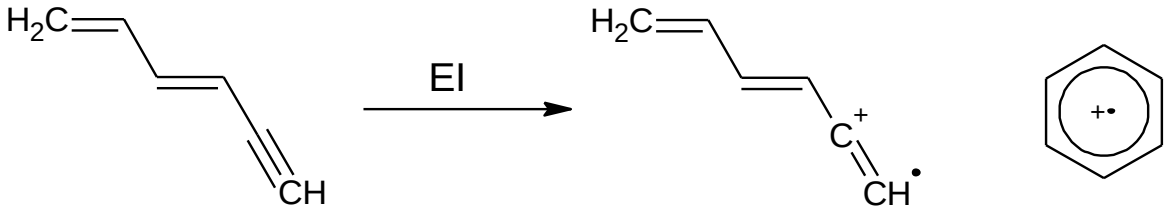

60% 40%

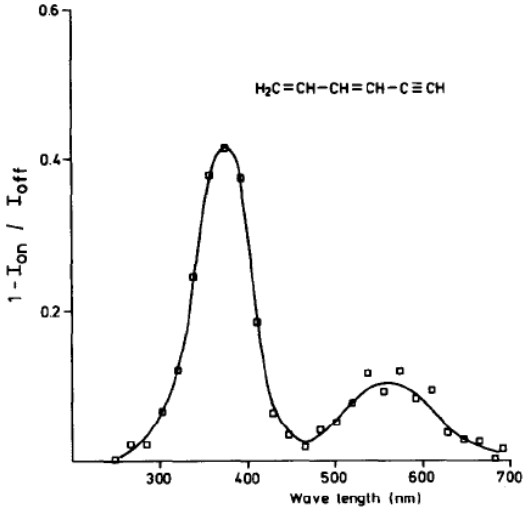

Fig. 6. Photodissociation spectrum of $m/z = 78$ ions from 1,3-hexadien-5-yne at a pressure of 7×10^{-7} Pa and an irradiation time of 2 s.

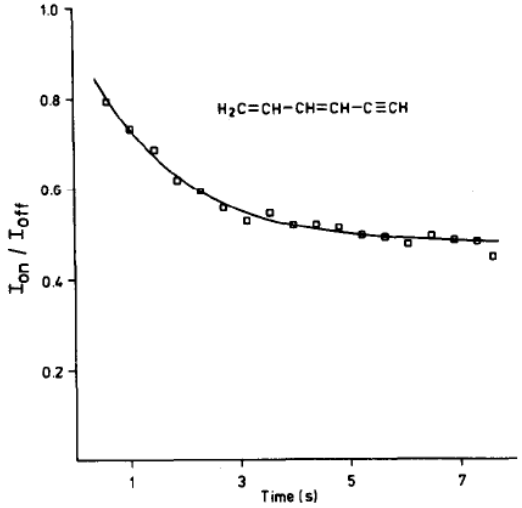

Fig. 7. Photodissociation time plot of $m/z = 78$ ions from 1,3-hexadien-5-yne at 7×10^{-7} Pa and a wavelength of 375 nm.

W.J. van den Haart et al. *Int. J. Mass Spectrom. Ion Proc.* **72** 99 (1986)

Tunable UV and FT-ICR

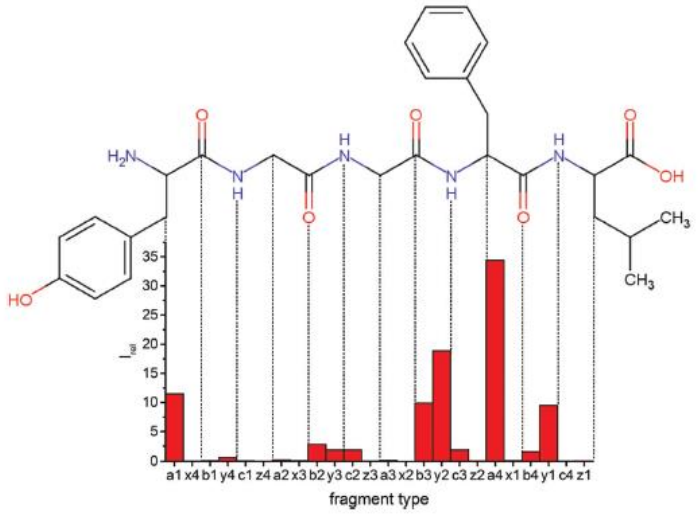

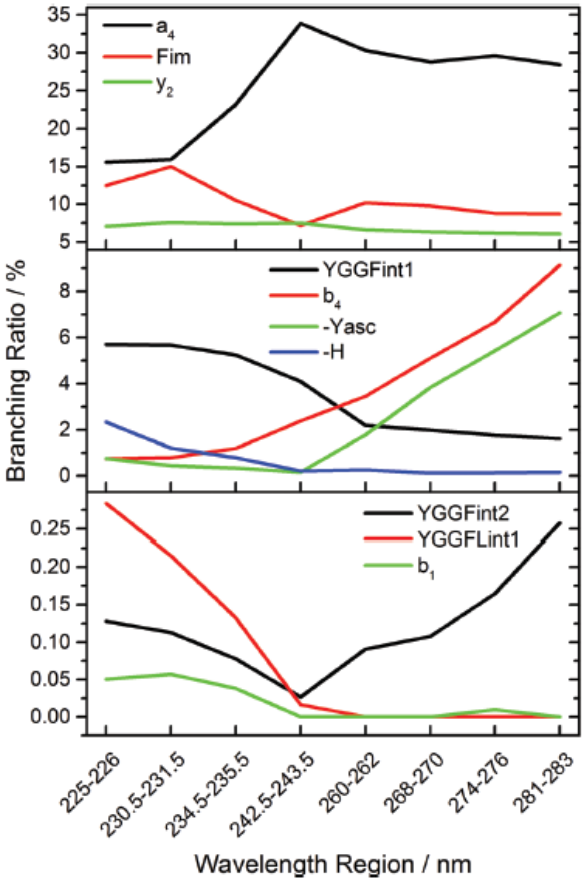

- Fragmentation favored close to the aromatic residues.
- Some dependence of the pathways on the laser wavelength.

A. Herburger, C. van der Linde, M. Beyer, Phys. Chem. Chem. Phys. **19** 10786 (2017)

Tunable UV-PD

- FT-ICR trap is quite ideal for alignment with a laser and long activation periods due to a low photon flux.

Validation on small systems: flavin co-factors of flavoproteins

OPO UV-Vis laser @ Ecole Polytechnique

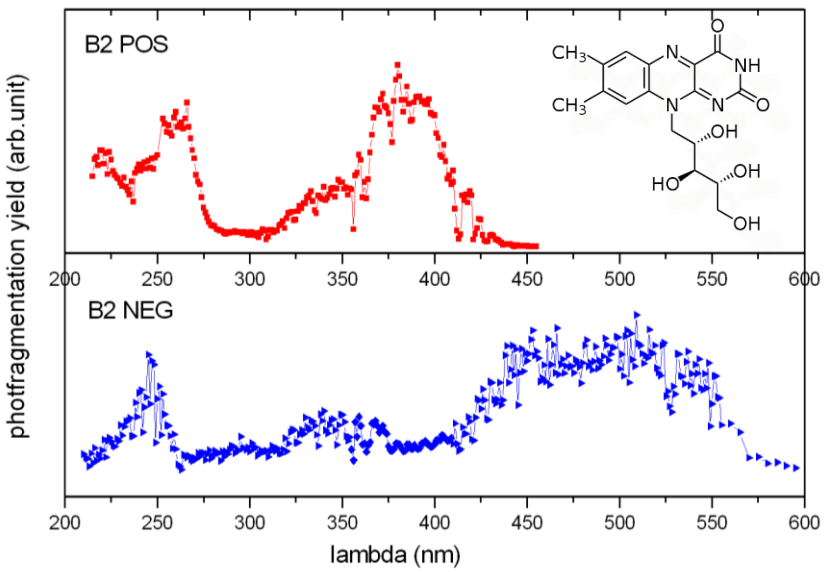

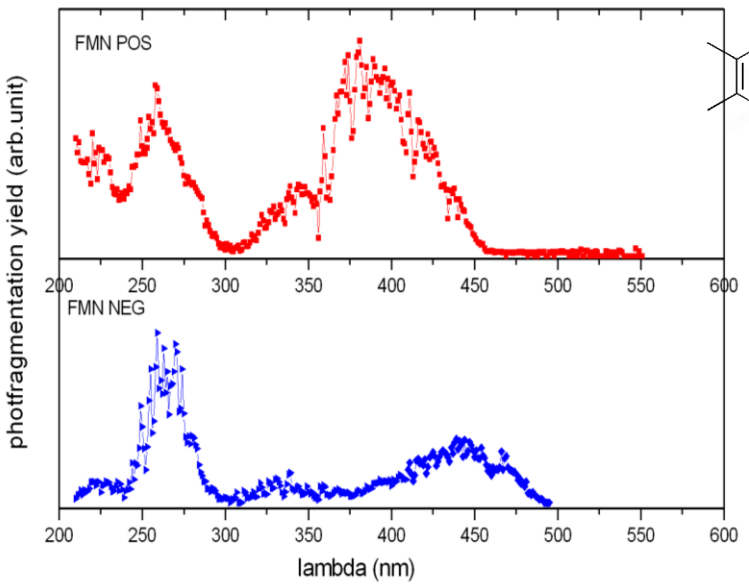

The optical response depends on the **chemical environment**

The optical response depends on the **charge environment**

UVPD at 213 nm in an FT-ICR

Check for updates

Cite this: *Analyst*, 2021, **146**, 3977

Influence of protein ion charge state on 213 nm top-down UVPD†

Simon Becher,[a] Huixin Wang,[b] Michael G. Leeming,[c] William A. Donald [d] and Sven Heiles *[a]

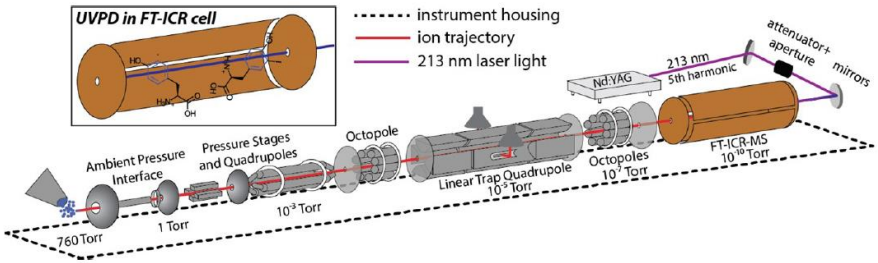

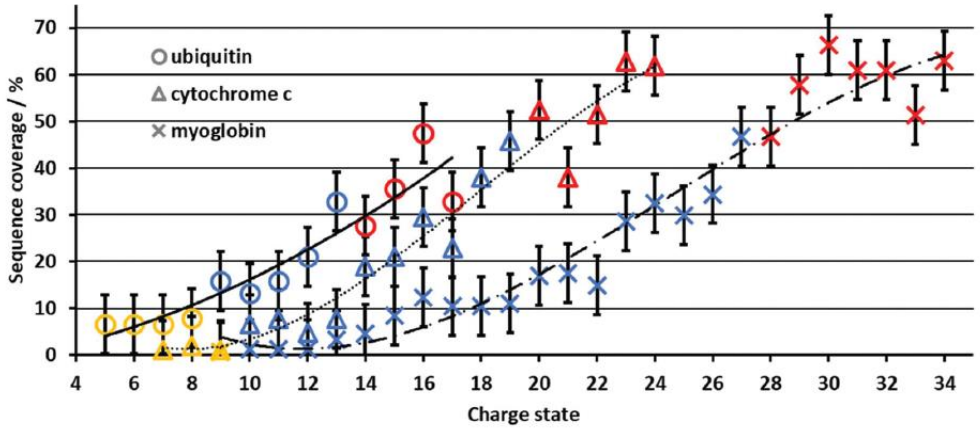

Fig. 2 Sequence coverage for ubiquitin, cytochrome c and myoglobin ions as a function of precursor charge state. Ubiquitin, cytochrome c and myoglobin are represented by circles, triangles and crosses, respectively. Proteins formed from native, denaturing and supercharging solutions are colored yellow, blue and red, respectively. The black lines serve as a guide to the eye.

UVPD – 193 nm allows protomer discrimination

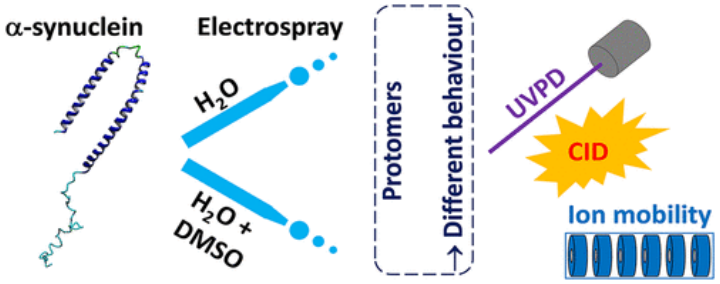

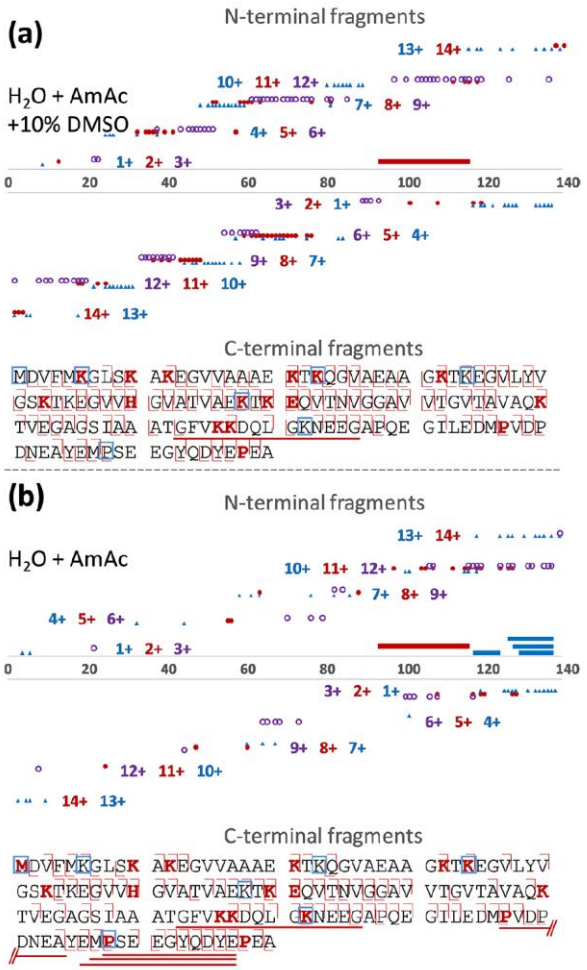

Figure 4. Cleavage sites and fragment charge states observed in UVPD of $[\alpha SN+14H]^{14+}$ sprayed from (H_2O + AmAc) or (H_2O + AmAc + 10% DMSO) and measured on the solariX instrument (triangles: 1+/4+/7+/10+/13+; filled circles: 2+/5+/8+/11+/14+; hollow circles: 3+/6+/9+/12+). N- and C-terminal fragments were aggregated across (*a*-, *b*-, *c*-) and (*x*-, *y*-, *z*-) type fragments. Cleavage coverage was 63.3% without and 77.0% with addition of DMSO. Internal fragments are displayed as horizontal lines underneath the sequence, and residues likely to carry a charge are in bold red text, with differences in charge sites between the two conditions indicated by blue boxes. In cases where cleavage coverage was insufficient to allow us to pinpoint charge to a single residue, the most likely residues, based on basicity, are displayed in bold red, leading to slightly more residues (16 and 17, respectively) than charges being labelled. Spectra used to generate this figure are shown in Supporting Information Figure S6. A similar analysis, based only on *a*-type fragments, yields very similar results, with the main difference being a shift of the P(117) proton to K(102)/E(104) in the absence of DMSO, possibly indicating that this is mobilized during *b*/*y* ion formation (Supporting Information Figure S7).

F. Lermyte, A. Theisen, P.B. O'Connor, *J. Am. Soc. Mass Spectrom.* **32** 364 (2021)

UVPD at 213 nm in an FT-ICR

Check for updates

Cite this: *Analyst*, 2021, **146**, 3977

Influence of protein ion charge state on 213 nm top-down UVPD†

Simon Becher,[a] Huixin Wang,[b] Michael G. Leeming,[c] William A. Donald [d] and Sven Heiles *[a]

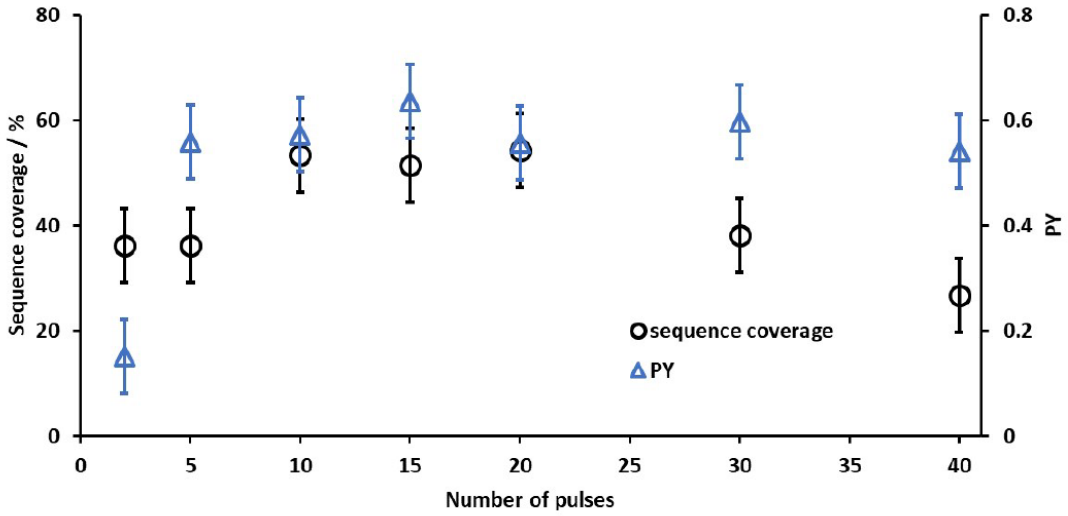

Figure S5. Sequence coverage (black circles) and PY (blue triangles) of [cytochrome c+19H]$^{19+}$ as a function of the number of laser shots per spectrum.

Drop in sequence coverage attributed to the fragmentation of fragments.

This is also an issue for other approaches with multiple photon processes.

Femto-second laser induced dissociation

Technique introduced by G.E. Reid in 2009 for peptide fragmentation analysis, using an activation in a rf ion trap device.
No absorption band is required (due to the extremely high electric field generated in the impulse).

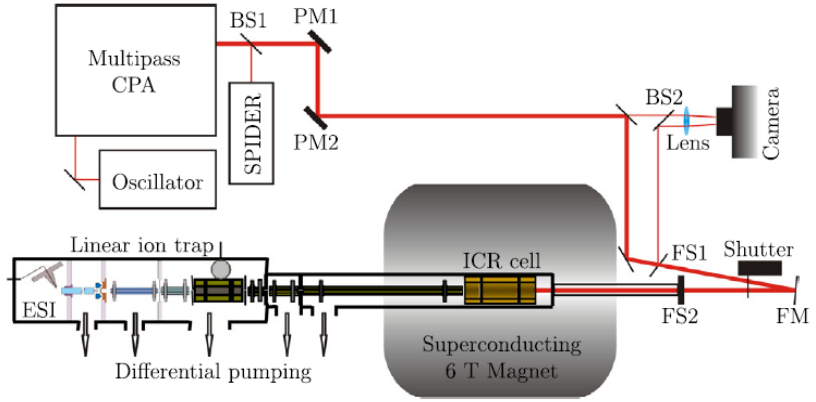

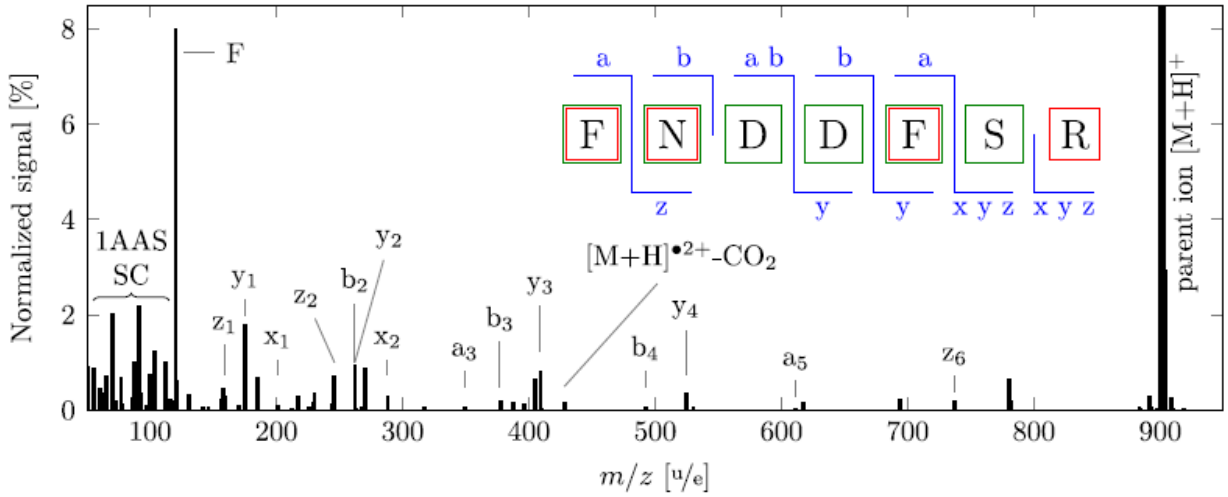

C. Neidel et al. Chem. Phys. (2018)

MULTIPLE PHOTON PROCESSES

Multiple photon processes in the Visible range

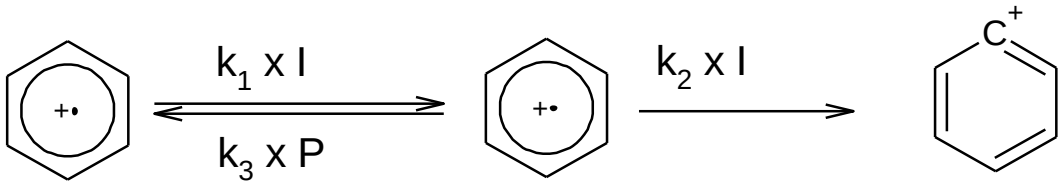

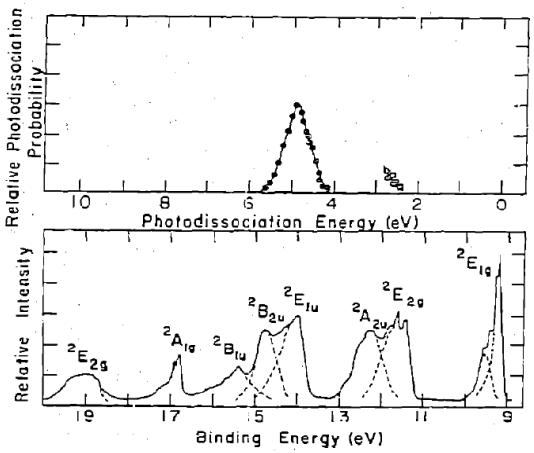

Fig. 1. Comparison of the deconvoluted photoelectron spectrum of benzene to the partial photoexcitation function for the two photon process, obtained using eight argon ion laser lines between 4545 Å and 5145 Å (o), and the complete excitation function for the direct process at 50 Å resolution (•). The energy axis of the photoelectron spectrum is adjusted such that the first adiabatic ionization potential of benzene is zero on the photodissociation energy scale. The relative photodissociation probability for the one and two photon processes are not directly comparable.

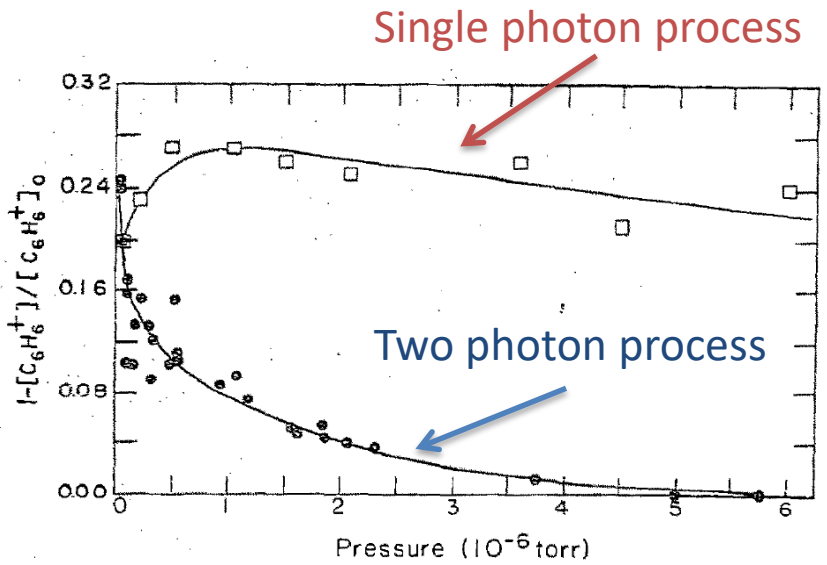

B.S. Freiser, J.L. Beauchamp, Chem. Phys. Lett. **35**, 35 (1975)

Infra-red Multiphoton dissociation

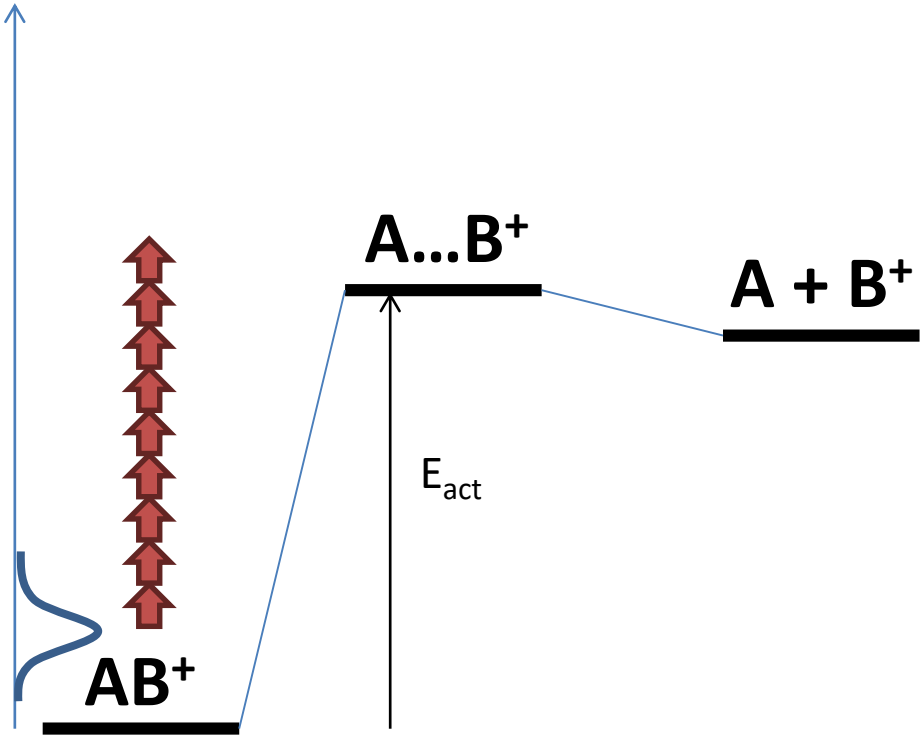

Multiple photon activation:

- IR photon ~ 0,1 eV
- Absorption of a number of photons is required to lead to fragmentation ***I**nfra-**R**ed **M**ulti-**P**hoton **D**issociation (IRMPD)*

- As for UVPD, an absorption band is required to observe fragmentation.

Wavelength ranges in IR spectroscopy

O-H / N-H stretches
Influenced by H-bonding

C-H stretches

Fingerprint region

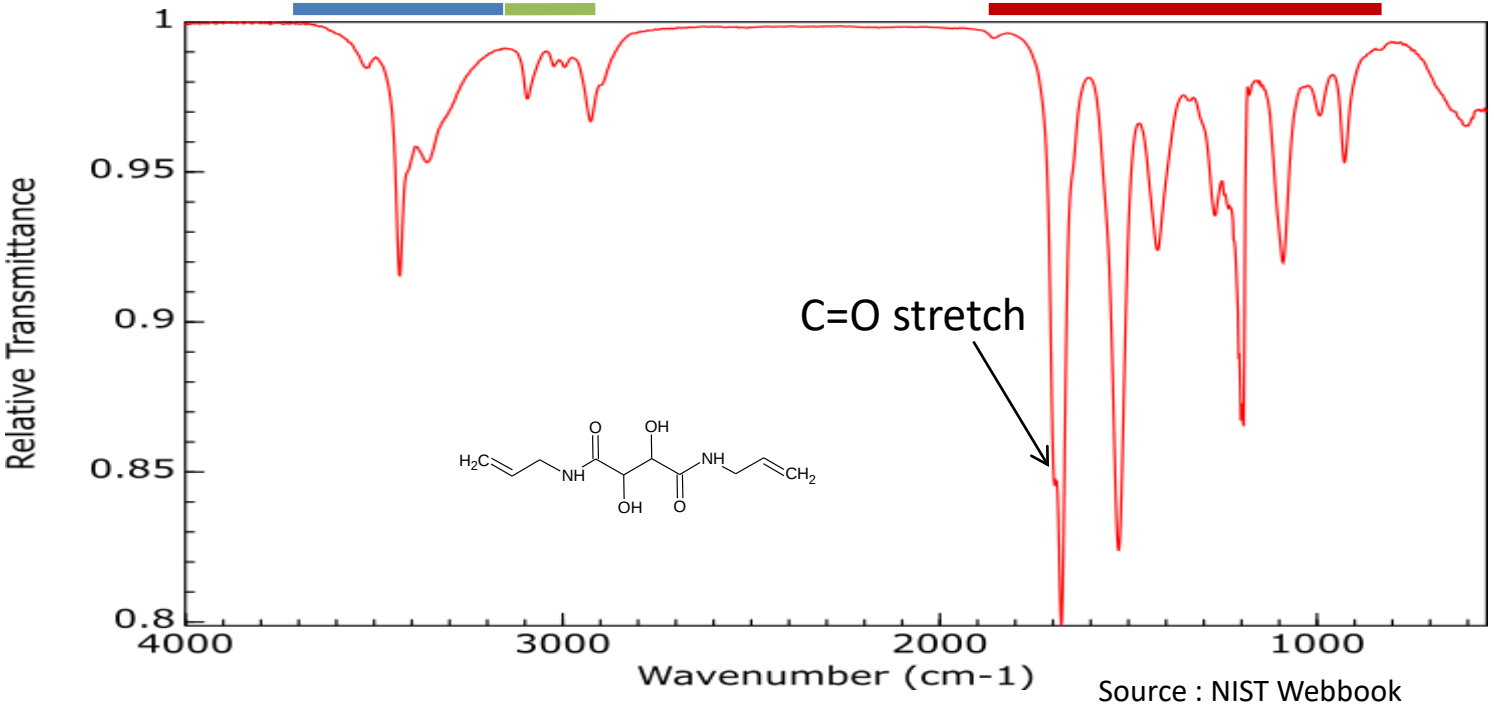

Source : NIST Webbook

Photon sources for IRMPD

- Tunable lasers – Free Electron lasers

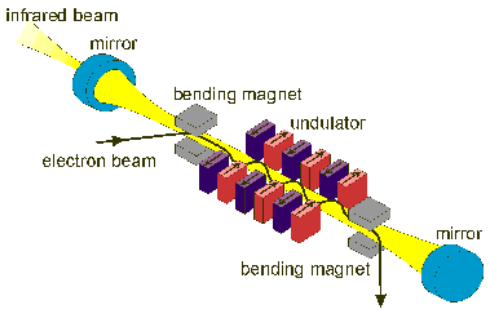

Based on an electron accelerator (16-48 MeV)
IR beam is generated within the undulator placed in the optical cavity.

Tuning of the wavelength by adjusting the gap between two sets of magnets in the undulator.

At 40 MeV : access to the 800-2000 cm-1 band (Fingerprint region) with ~1 W of power.

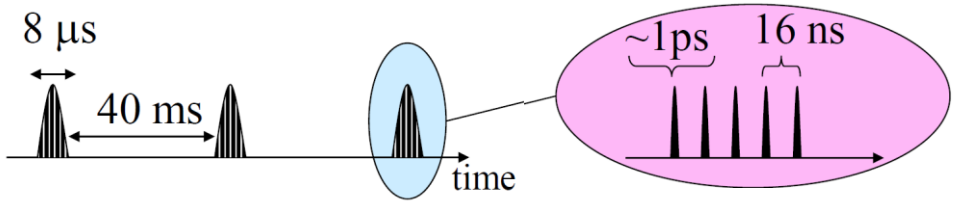

Photon sources for IRMPD

- Tunable lasers : table-top OPO-OPA lasers

  Based on the non-linear optical properties of crystal materials (such as KTP potassium titanyl phosphate)

  Repetition rate: 10 – 25 Hz, Power: ~10 mJ.

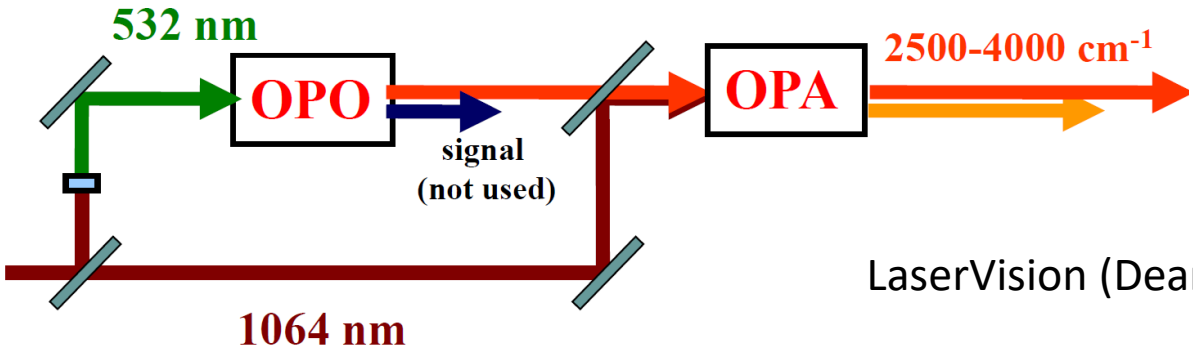

LaserVision (Dean Guyer)

Optical Parametric Oscillator Generates signal

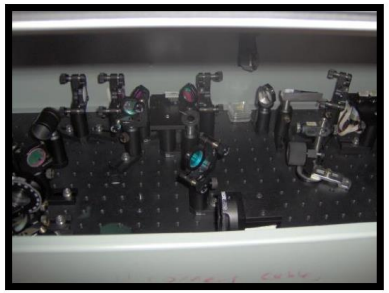

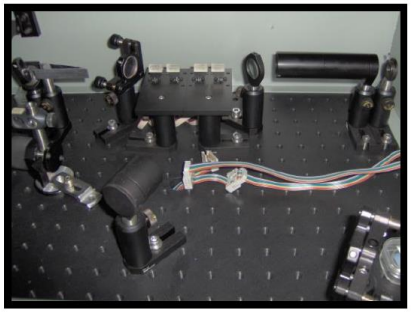

Optical Parametric Amplifier Boosts signal (single pass)

Photon sources for IRMPD

- CO_2 laser

- Electric discharge in a N_2 / CO_2 / He gas mixture
- High power conversion efficiency (up to 20%)
- High power (50 W or more can be purchased readily)
- Fixed wavelength (some are tunable) between 10.6 µm and 9.4 µm.

Principles of IRMPD

IVR : statistical redistribution of energy in several vibration modes of the molecule

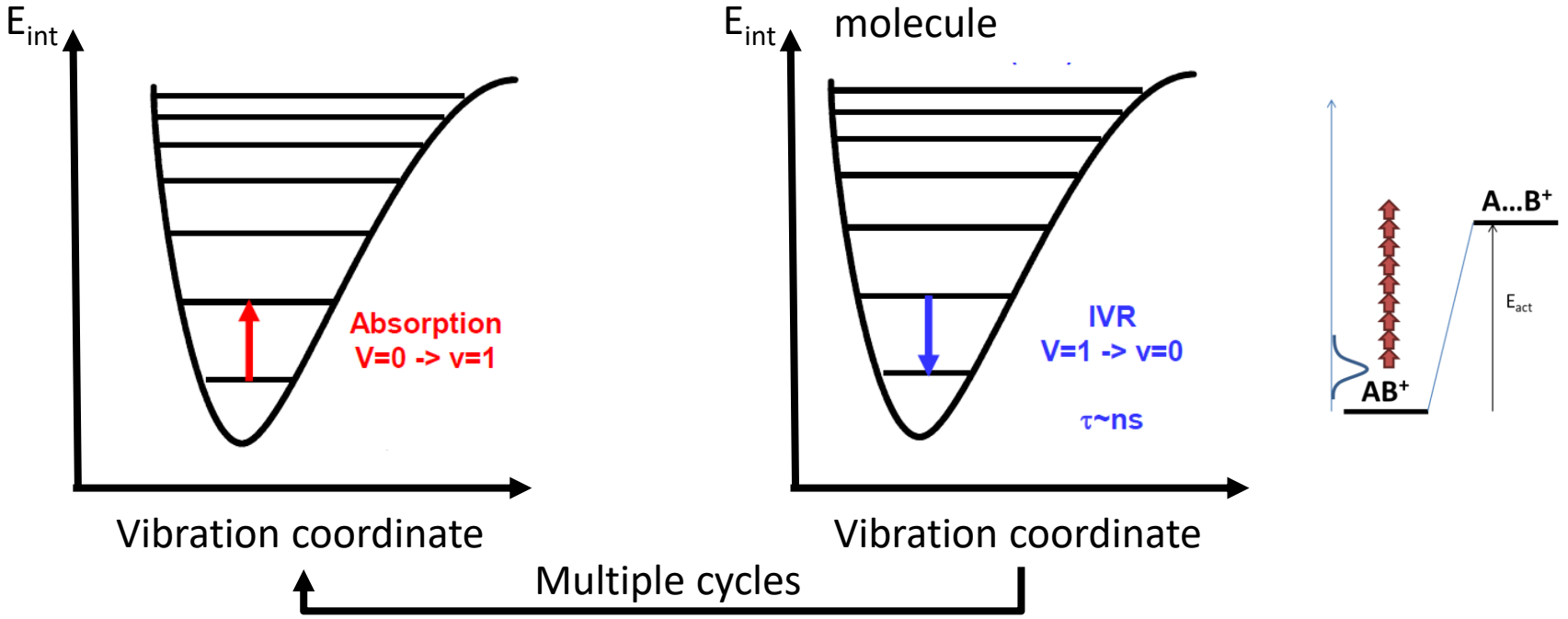

Referring to IRMPD : « This method employs an intense infrared laser to resonantly pump vibrational energy into the molecule in a **noncoherent** fashion, until it has sufficient energy to dissociate. »

R. C. Dunbar, D. T. Moore, J. Oomens, *J. Phys. Chem. A* **110**, 8316-8326 (2006)

Advantages of FT-ICR for IRMPD spectroscopy

- Multiphoton process can be inhibited by collisional relaxation.
  - In ion traps, relaxation occurs within 10 ms (P.M. Remes, G.L. Glish J. Am. Soc. Mass Spectrom. **20**, 1801 (2009)) which is shorter than the time between two OPO laser pulses or two FEL macropulses.
  - FT-ICR vacuum is thus better suited for IRMPD when a single pulse is not sufficient to accumulate sufficient amount of energy in an ion trap.
    - Many benefits for :
      - Large molecular systems (increased kinetic shift)
      - Strongly bound systems
      - Low intensity bands (but requires multiple passes and spectrum stiching).
    - Ion trap present the option of ion tagging as a subtitute for this limitation. But ion tagging can induce molecular structure shifts.

IRMPD spectroscopy in practice

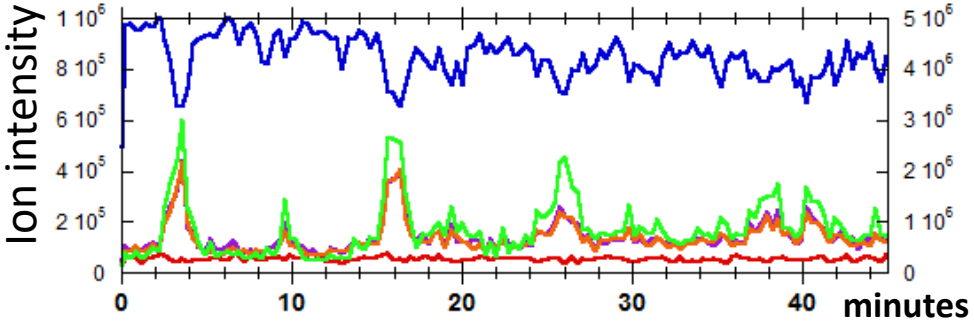

Spectrum recorded as an MS/MS chromatogram where each data point corresponds to one wavelength.
Synchronisation through instrument / laser TTL exchanges.

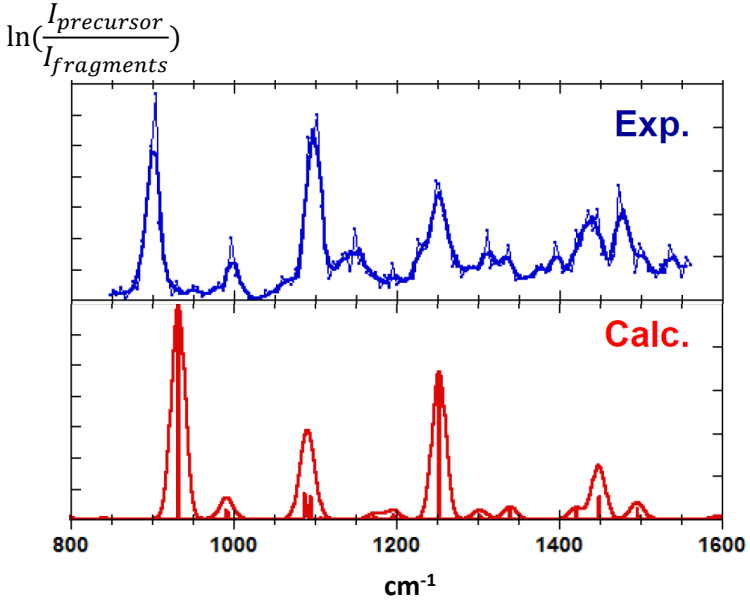

Comparison with calculated spectra

- Geometry optimization, mostly carried out with a standard basis set (6-31+G**)
  - Search for conformers with the lowest energy.
  - Harmonic bands are calculated from a frequency calculation and convoluted with a Gaussian profile (FWHM 10 or 20 cm^{-1})
- Scaling factors :
  - Multiple scaling factors have been proposed in the litterature depending on the method and basis set.
  - Issue is that most of the time the scaling factors differ between the fingerprint and harmonic regions (0.98 for fingerprint, 0.955 for X-H stretching region.

Scaling factors for IRMPD

- In 2017, we introduced the use of a linear scaling factor based on a series of 68 experimental values in the fingerprint region for which frequency assignment was structurally and spectrally unambiguous.
- The publication also introduces a measurement for similarity (similar to a Fisher test) which relies on the observed correlation for individual spectra.

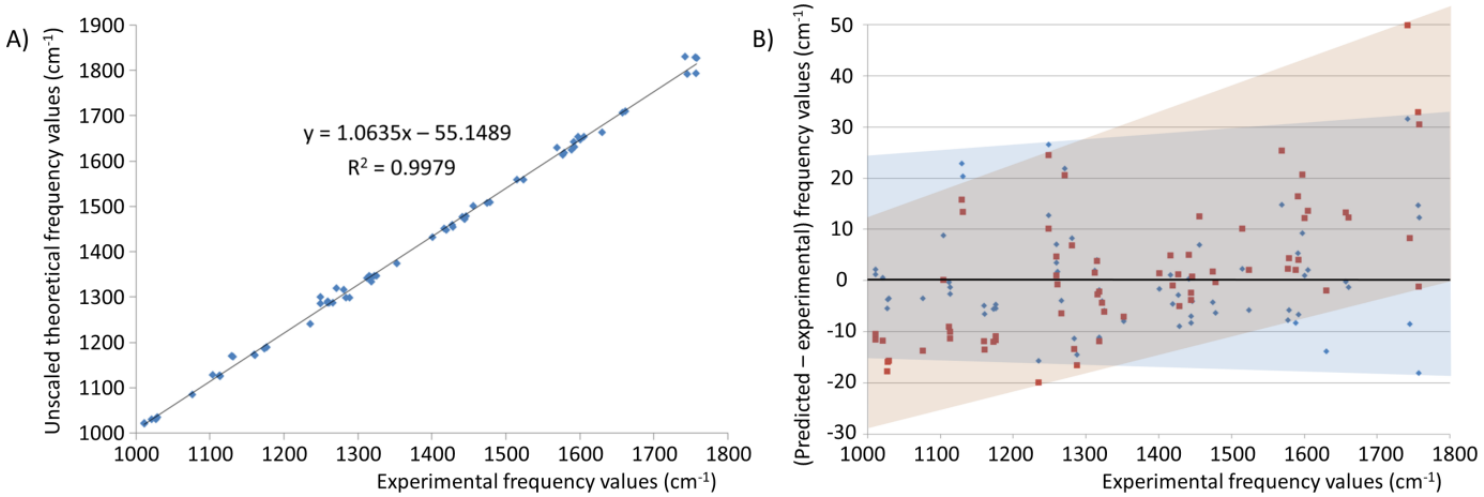

K. Madanakhrishna et al. Chem. Eur. J. **23**, 8414 (2017)

Improving OPO dissociation using CO_2 laser

- Low power of OPO laser can lead to situation in which radiative cooling exceeds resonant photoexcitation.
- CO_2 laser is synchronized with the OPO and irradiation time needs to be optimized for each system to set irradiation time just below the dissociation threshold.

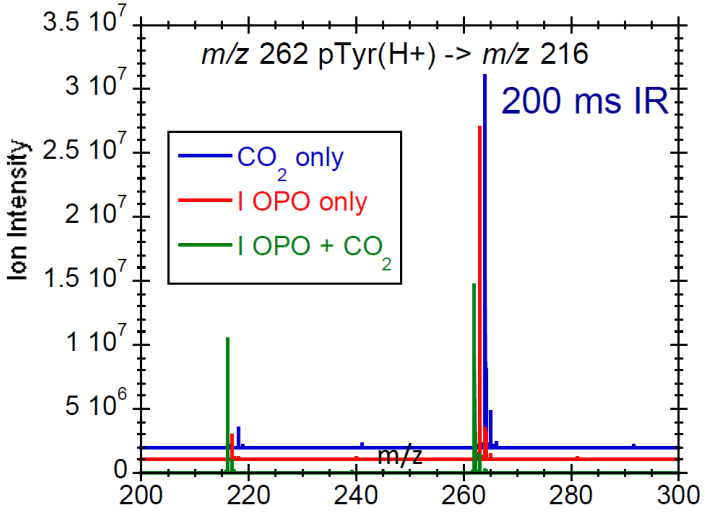

Phosphotyrosine+H⁺ : [pTyr+H]⁺

OPO, on resonance with an O-H band

OPO+CO_2: significant amplification

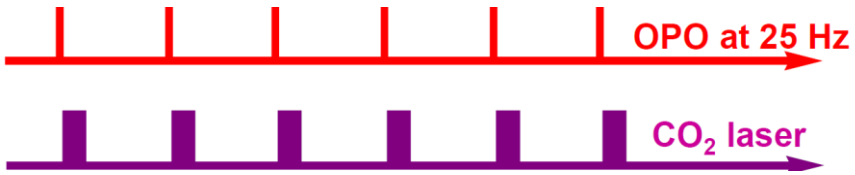

IRMPD at fixed wavelength

- Usually low intensity absorption bands in the fingerprint region at 943 cm^{-1}.
- High laser power (high photon density) compensates for the low intensity of the bands.

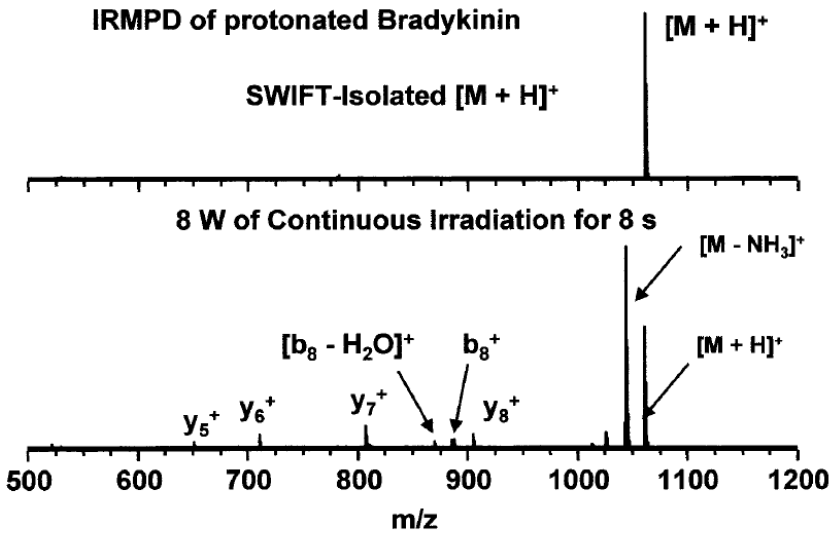

Figure 1. Infrared multiphoton dissociation (IRMPD) of protonated bradykinin, $[M+H]^+$. Protonated bradykinin was SWIFT-isolated (top) and irradiated with the IR laser for 8 s at 8 W (bottom).

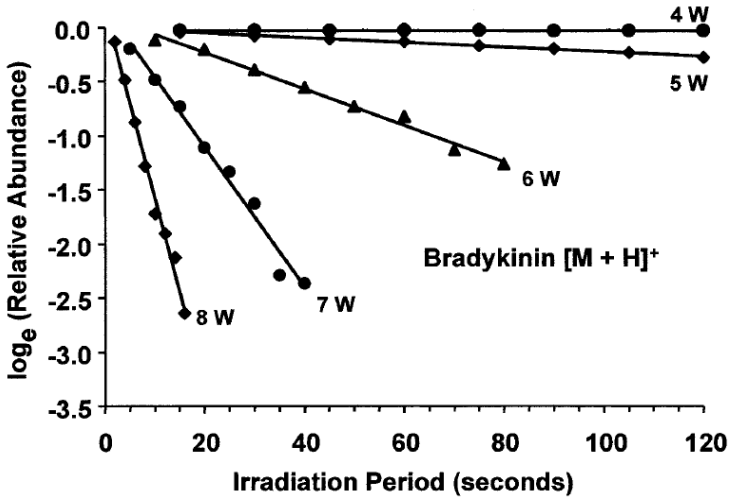

Figure 2. Plot of the natural logarithm of the relative abundance of protonated bradykinin, $[M+H]^+$, vs. time for unimolecular dissociation at each of five indicated laser powers. Note the highly linear behavior, showing that ions remain within the cross-section of the laser beam throughout the experiment.

M.A. Freitas et al. Rapid Comm. Mass Spectrom. **13**, 1639 (1999)

Resonant IRMPD with CO_2 laser

- Brodbelt and coworkers introduced the use of resonant IRMPD for phosphorylated peptides.

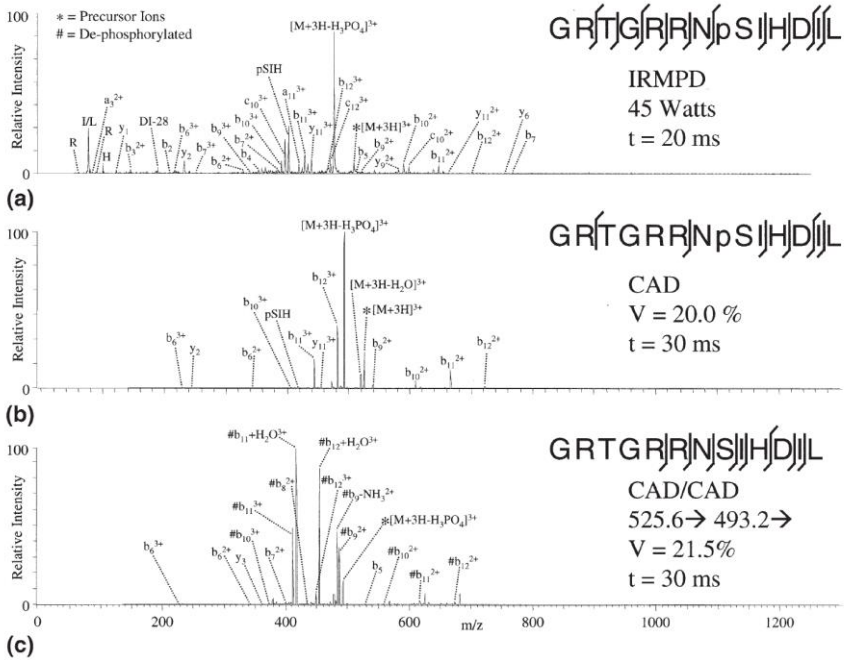

Figure 7. (a) IRMPD, (b) CAD MS^2, and (c) CAD MS^3 mass spectra of triply protonated GRT-GRRNpSIHDIL.

M.C. Crowe and J.S. Brodbelt, *J. Am. Soc. Mass Spectrom.* **15**, 1581 (2004)

Resonant IRMPD with CO_2 laser

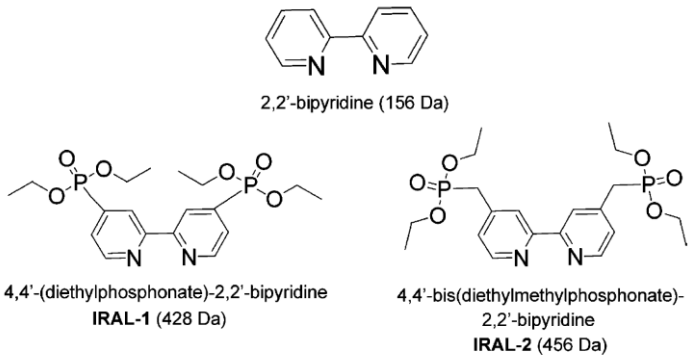

Figure 1. IR-active ligands based on the 2,2′-bipyridine skeleton synthesized and used in the study. Molecular weight is shown in parentheses.

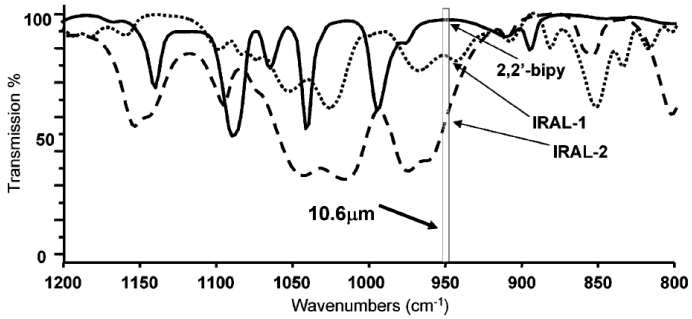

Figure 6. FTIR ATR spectra of the ligands used in the study, showing the enhanced absorption of the IR-active ligands, IRAL-1 and IRAL-2, at 10.6 μm as compared to 2,2′-bipyridine.

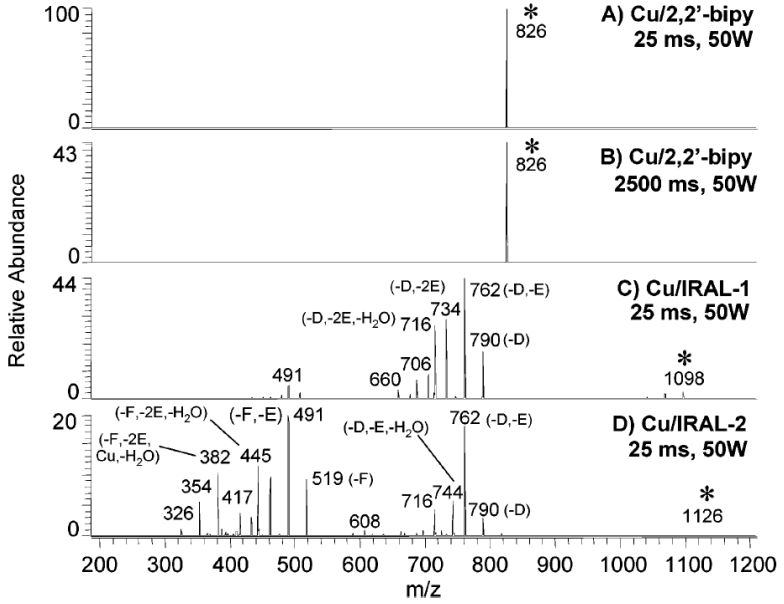

Figure 4. Irradiation of the $[Cu^{2+}(\text{neodiosmin} - H)\text{auxiliary ligand}]^+$ complexes containing different ligands: (A) $[Cu^{2+}(\text{neodiosmin} - H)2,2\text{-bipy}]^+$, 50 W for 25 ms; (B) $[Cu^{2+}(\text{neodiosmin} - H)2,2\text{-bipy}]^+$, 50 W for 2500 ms; (C) $[Cu^{2+}(\text{neodiosmin} - H)\text{IRAL-1}]^+$, 50 W for 25 ms; (D) $[Cu^{2+}(\text{neodiosmin} - H)\text{IRAL-2}]^+$, 50 W for 25 ms.

M. Pikulski et al. *Anal. Chem.* **78**, 8512 (2006)

Resonant excitation with tunable IR laser

- Peptide fragmentation has been abundantly studied using IRMPD spectroscopy.

b and a type ions have electrophilic and nucleophilic groups : cyclisation during the fragmentation process is an option.

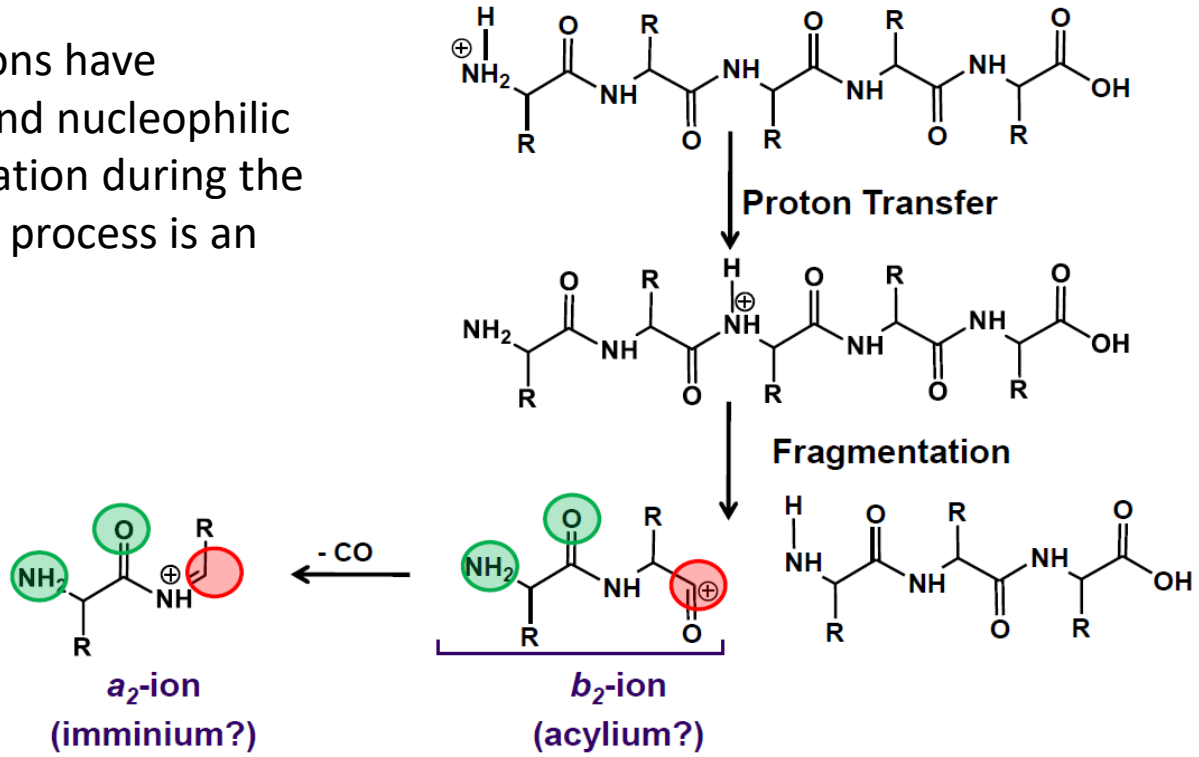

Peptide structures solved through tunable IRMPD

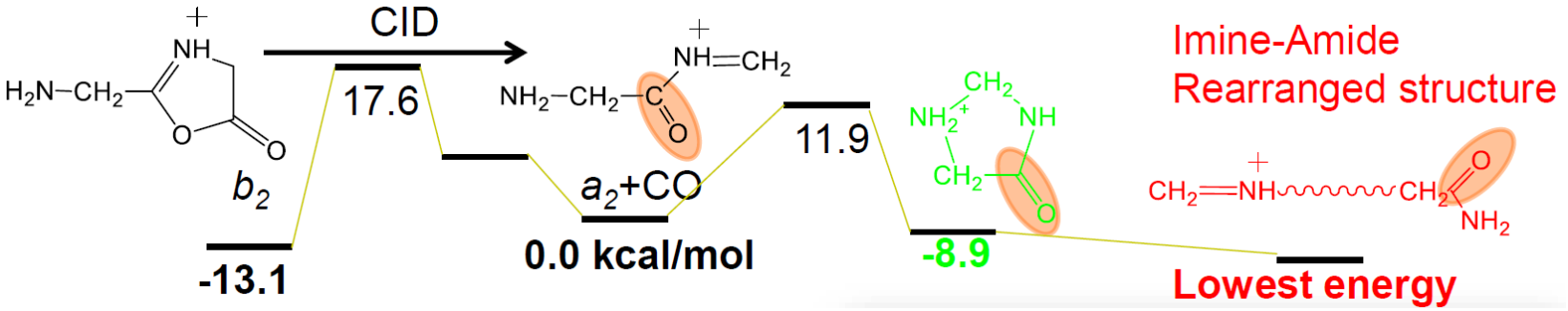

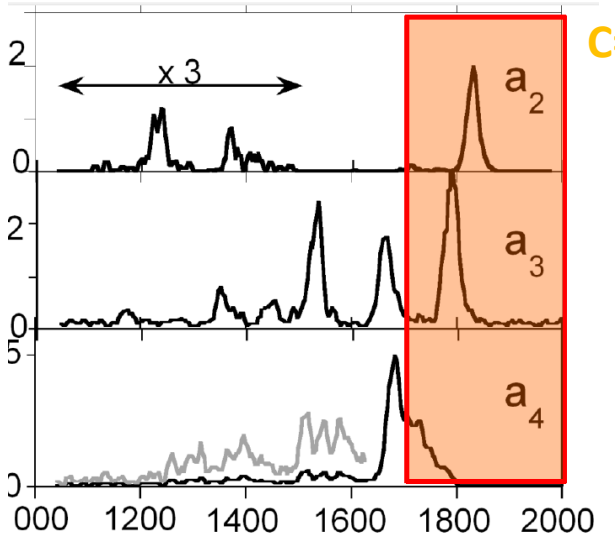

C=O stretch region

Oligoglycine a_2, a_3 and a_4 ions display strongly different C=O stretches.
Rearrangement of the a_n ions is kinetically controlled.

B. Bythell et al. J. Am. Chem. Soc **132**, 14766 (2010)

Peptide structures solved through tunable IRMPD

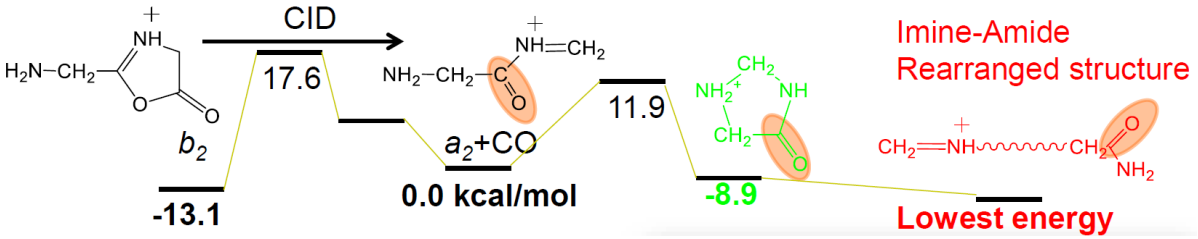

Example of the a_2 ion

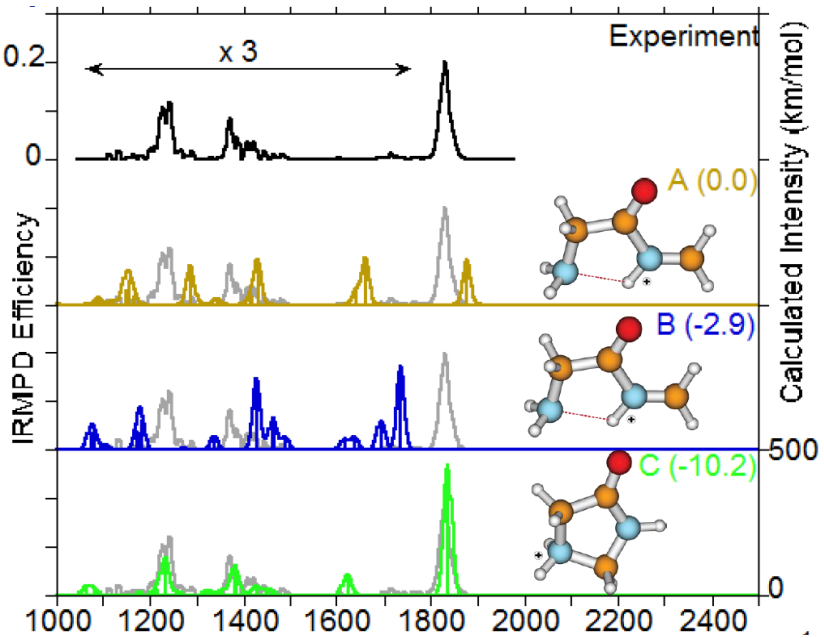

B. Bythell et al. J. Am. Chem. Soc **132**, 14766 (2010)

Peptide structures solved through IRMPD spectroscopy

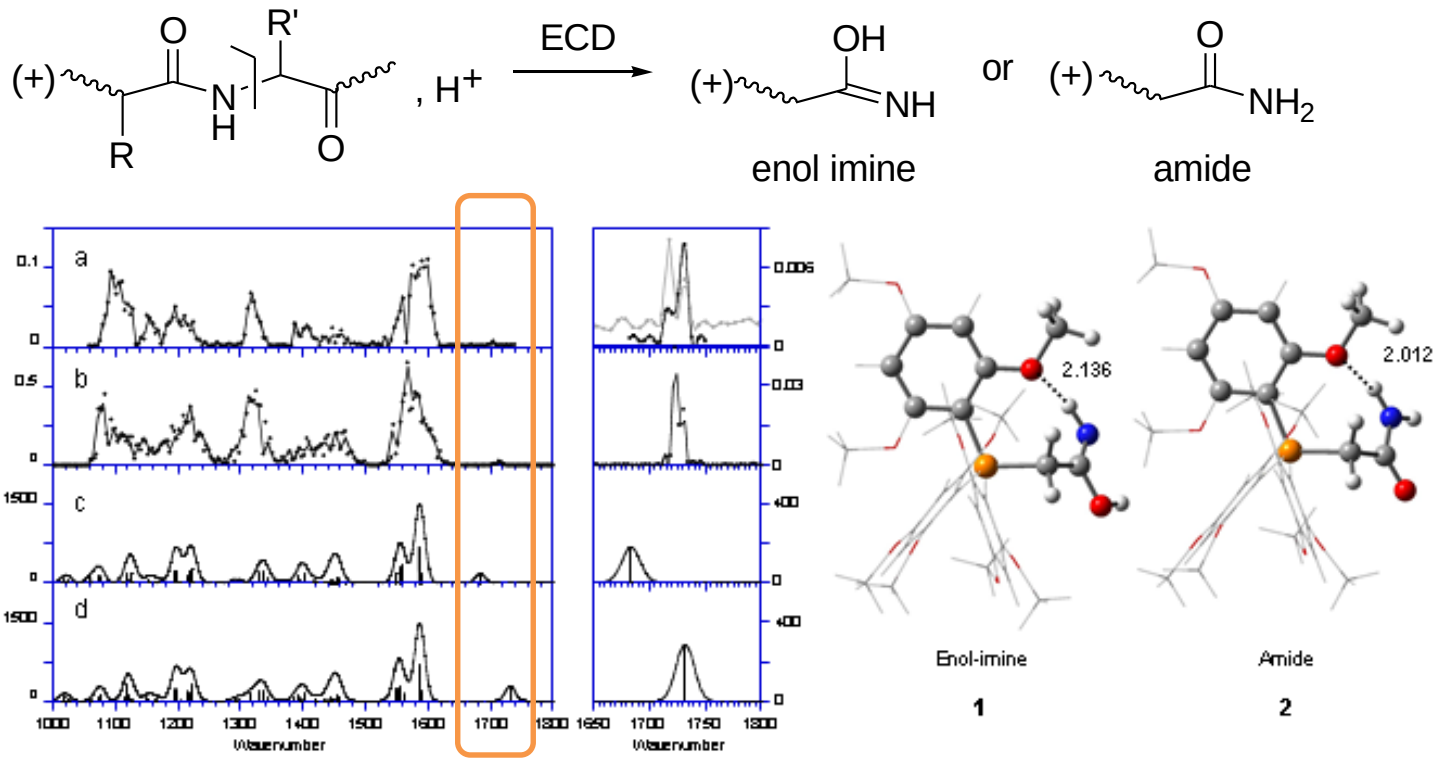

G. Frison et al. *J. Am. Chem. Soc.* ***130,*** 14916 (2008)

Organometalic systems

Several turn overs have been achieved under MS/MS conditions

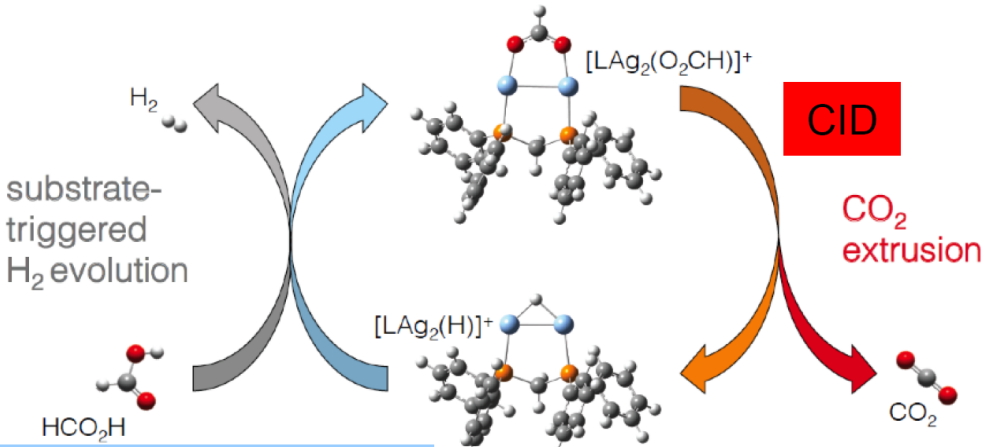

Ion-Molecule Reaction

Proposed catalytic cycle for $HCO_2H \rightarrow H_2 + CO_2$

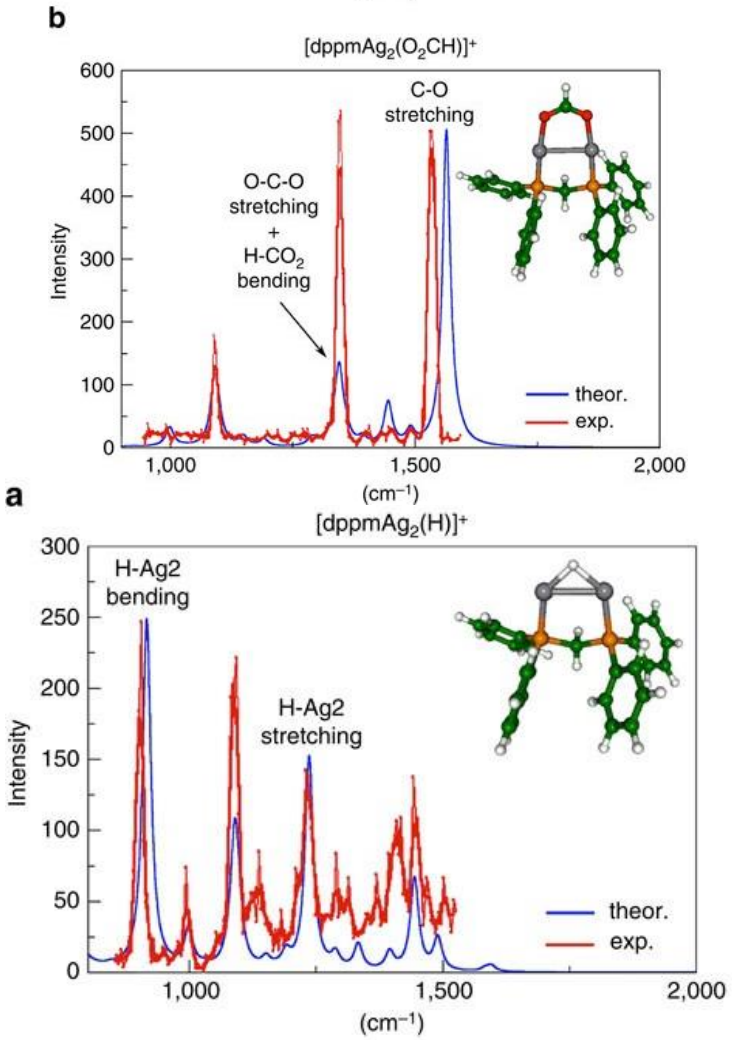

A. Zavras et al. *Nature Comm.* **7** 11746 (2016)

BIRD

- Radiative equilibrium between ions and cell walls.

Presure ~10^{-6}-10^{-8} mbar
t ~ 10s of seconds

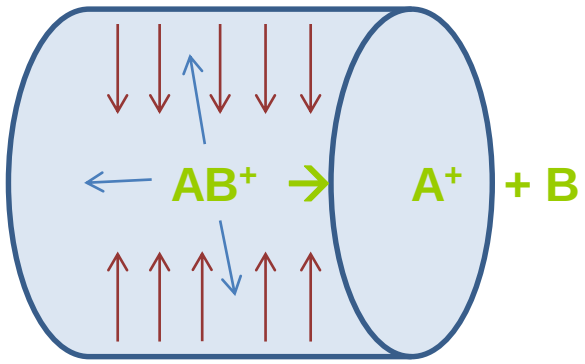

T_{walls}

Measurement of fragmentation kinetics at variable temperatures:

$$k(T) = A\, e^{-\frac{E_a}{RT}}$$

Access to kinetic parameters (A and E_a)

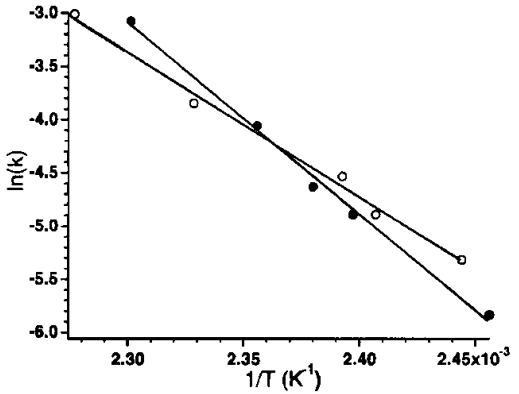

Figure 2. Arrhenius plot for dissociation of ubiquitin 5+ (○) (E_a = 1.2 eV; $A = 10^{12}$ s^{-1}) and 11+ (●) (E_a = 1.6 eV; $A = 10^{17}$ s^{-1}).

Application to a protein – ligand system

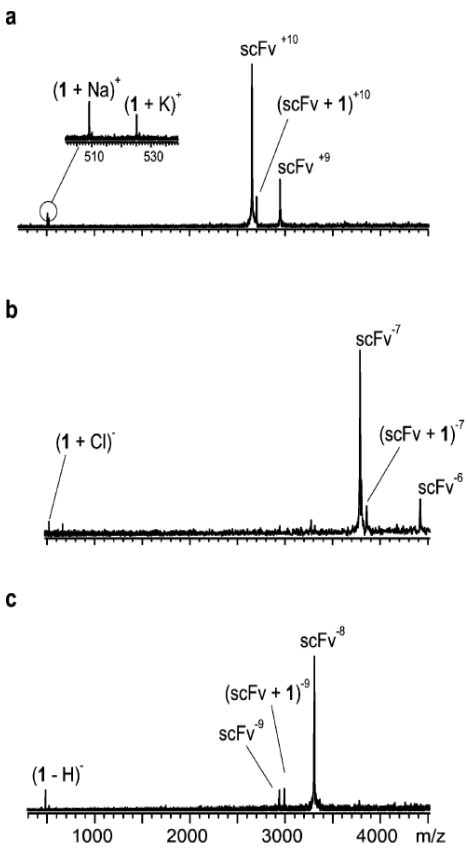

Figure 4. BIRD mass spectra obtained for protonated and deprotonated (scFv +**1**)$^{n+/-}$ ions (a) $n = +10$, 154 °C, 6 s; (b) $n = -8$, 147 °C, 5 s; (c) $n = -9$, 147 °C, 5 s.

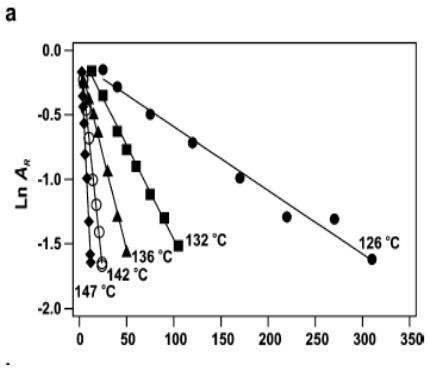

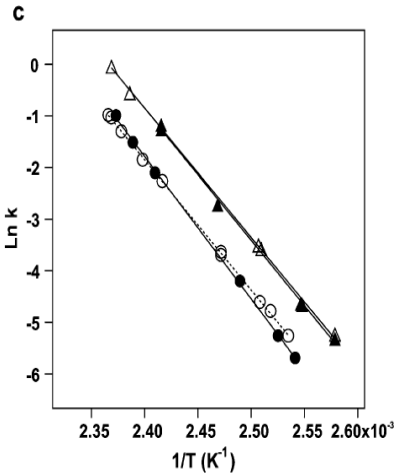

Figure 6. Arrhenius plots obtained for the loss of neutral L from the (P + L)$^{n+/-}$ ions: (a) L = **1**, P = scFv, +6 (◆), +7 (◇), +8 (△), +9 (▲), +10 (●), +11 (■), +12 (○), +13 (×), (b) L = **1**, P = scFv, −6 (□), −7 (▼), −8 (▽); (c) $n = +10$, L = **1**, P = scFv (●), L = **1**, P = His^{H101}Ala (○), L = **4**, P = scFv (▲), L = **4**, P = His^{H101}Ala (△).

E.N. Kitova et al, J. Am. Chem. Soc ***130****, 1214 (2008)*

Precursor ion activation

From here onwards: we are going to change not only the internal energy but also the chemistry!

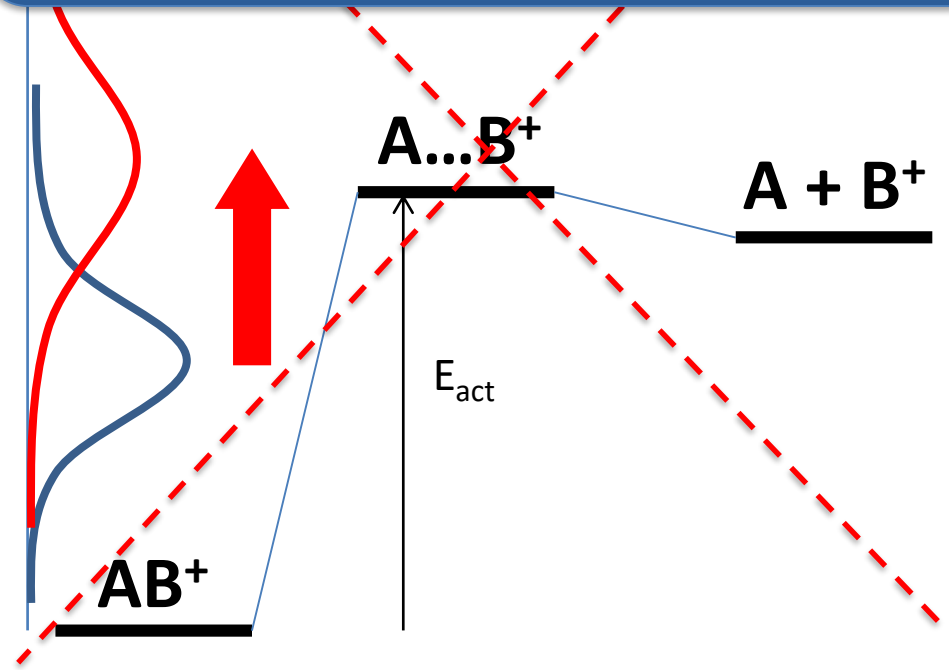

Activation methods:

Collision with an inert gas (CID)

Collision with a surface (SID)

Photon absorption :
UV (UVPD)
IR (IRMPD)

Reactive activations :

Reactive collisions with a gas
Cation / anion reaction
Interaction with electrons.

Ion-molecule reactions

- If one wants to study a reaction between an ion and a gas:

$$I^+ + N \rightarrow P^+ + R$$

- The FTICR cell will allow to trap ions for long and variables times and to measure reaction products.
- From the kinetics, one can derive rate constants. If the pressure of the neutral is known or measured through an other experiment, bimolecular rate constants can be derived.

Some examples of kinetics

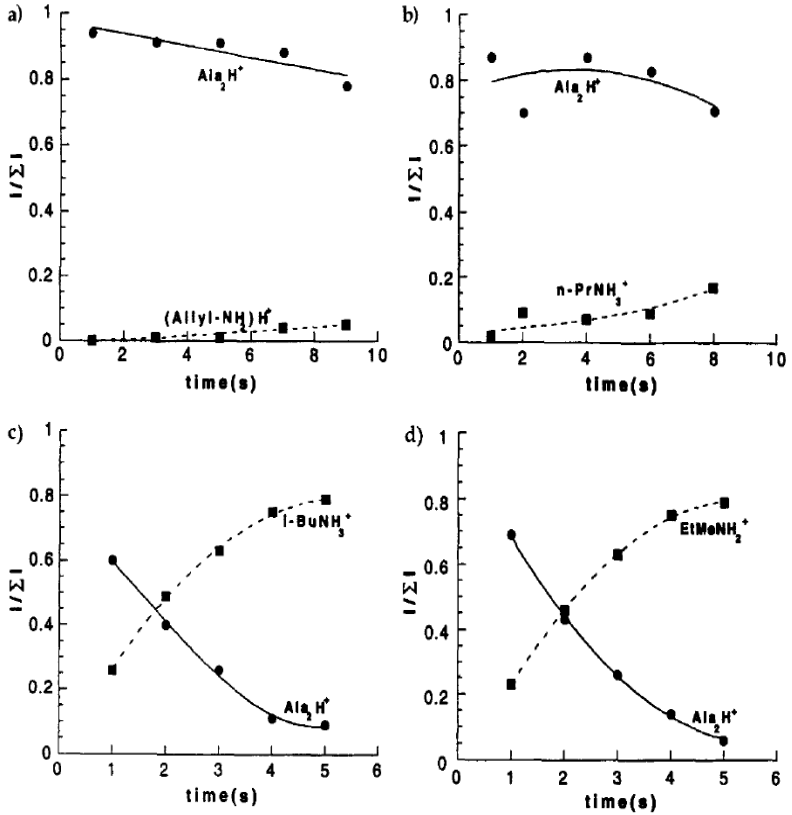

Figure 2. Relative intensity profile of protonated dialanine reacting with (**a**) allylamine, GB = 207.9 kcal/mol (1.4×10^{-8} torr), (**b**) *n*-propylamine, 210.1 (1.3×10^{-8} torr), (**c**) *i*-butylamine, 211.1 (1.2×10^{-8} torr), and (**d**) ethylmethylamine, 215.1 (1.1×10^{-8} torr). The symbol $I/\Sigma I$ represents the intensity of the ion over all ion intensities. No reactions or extremely slow reactions are observed in (a) and (b), whereas rapid reactions are observed in (c) and (d). The GB of dialanine therefore lies between the GB of *n*-propylamine and *i*-butylamine.

ORIGINS OF ELECTRON ACTIVATION TECHNIQUES

Variations on electron activation (ExD)

- Direct interaction with the electron flux

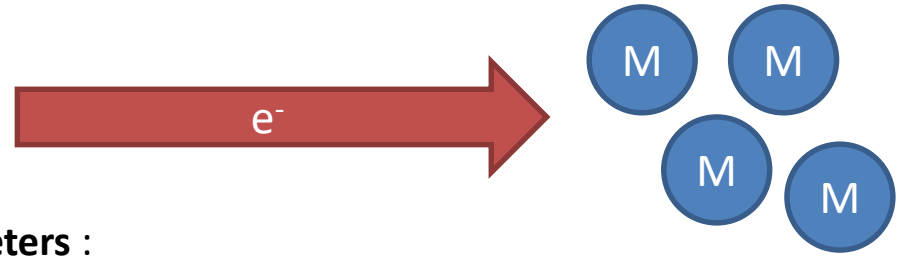

Parameters :

- Electron kinetic energy (eV), which plays on the interaction cross section and energy available in the system.
- Flux of the electron beam
- Irradiation time

- Electron transfer between two molecules

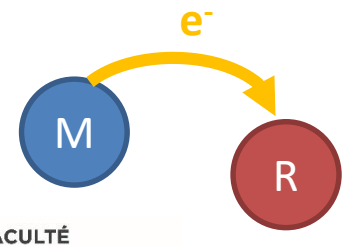

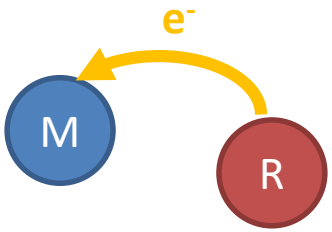

Origins of electron capture dissociation

ELSEVIER International Journal of Mass Spectrometry and Ion Processes 157/158 (1996) 357–364

193 nm photodissociation of larger multiply-charged biomolecules

Ziqiang Guan, Neil L. Kelleher, Peter B. O'Connor, David J. Aaserud, Daniel P. Little, Fred W. McLafferty*

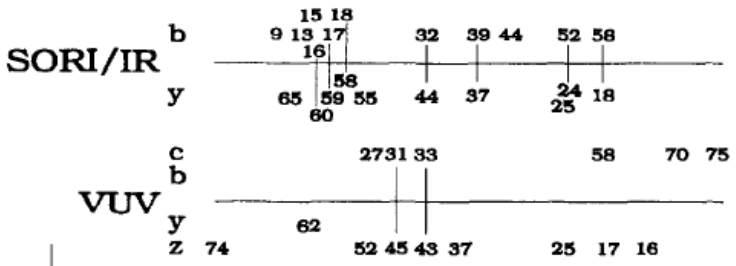

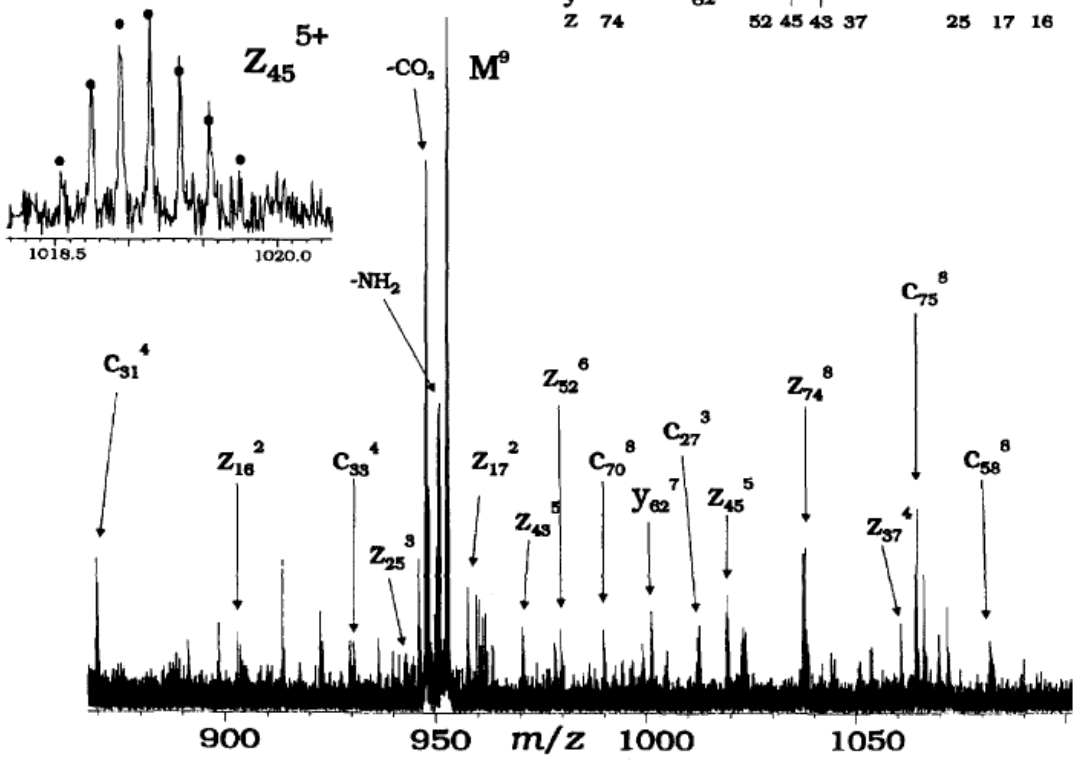

Before ECD was even conceived, the authors were marked by:

- Formation of *c* and *z* ions
- Fragmentation of large size systems

Formation of *c* and *z* ions

Electron Capture Dissociation of Multiply Charged Protein Cations. A Nonergodic Process

Roman A. Zubarev, Neil L. Kelleher, and Fred W. McLafferty*

J. Am. Chem. Soc. **1998,** *120,* 3265−3266

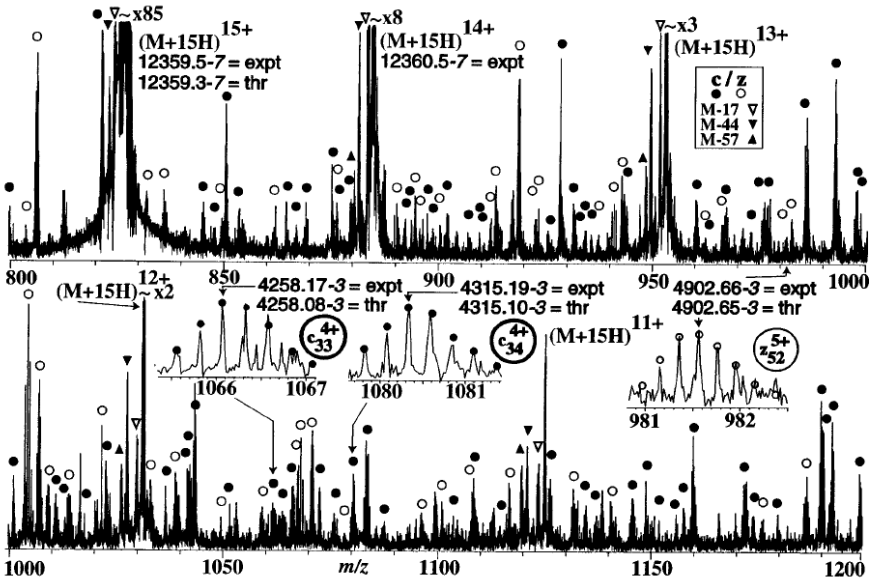

Figure 2. ECD spectra of 15+ ions of cytochrome *c* (Fe^{III}),[16] 75 scans: ∇, −17 Da; ▼, −44 Da; ▲, −59 Da; ●, *c* ions, ○, *z* ions. Mass values are for the neutral molecule's most abundant isotopic peak; the mass difference (units of 1.0034 Da) between this and the monoisotopic peak is shown by the italicized final digit.[6] Circles, as in Figure 1.

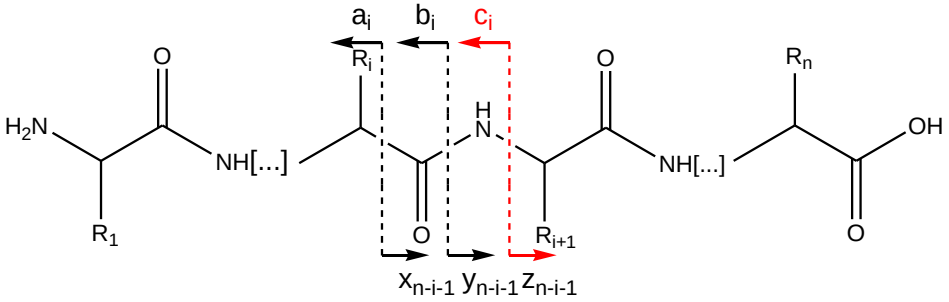

Dissociative recombination: one of the origins of ECD

- Started in the early 1980s.
- Mainly for systems of astrophysical or planetary interest.

$$M^{\bullet+} + e^- \rightarrow M^* \rightarrow N_1 + N_2$$

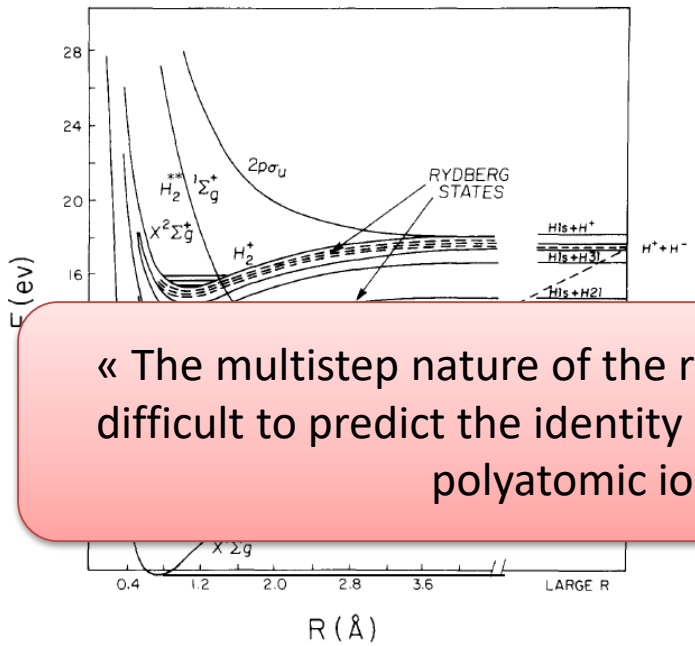

Theories elaborated for DR serve as a basis for the understanding of ECD:

- Direct capture in a dissociative state versus indirect capture in a Ryberg state
- Electron energy dependence in $1/E_c$

→ Requirement to work at low electron energy

« The multistep nature of the recombination process means that it is very difficult to predict the identity of the products. This is particularly true for polyatomic ions. » J.B.A. Mitchell, 1990

Review: Mitchell, *Physics Reports* 1990.

Some parallels with the much better known electron ionization

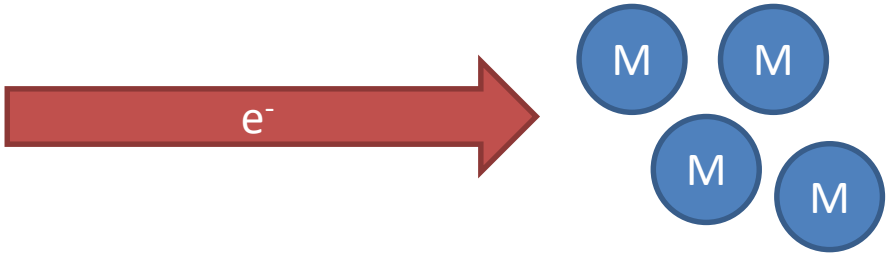

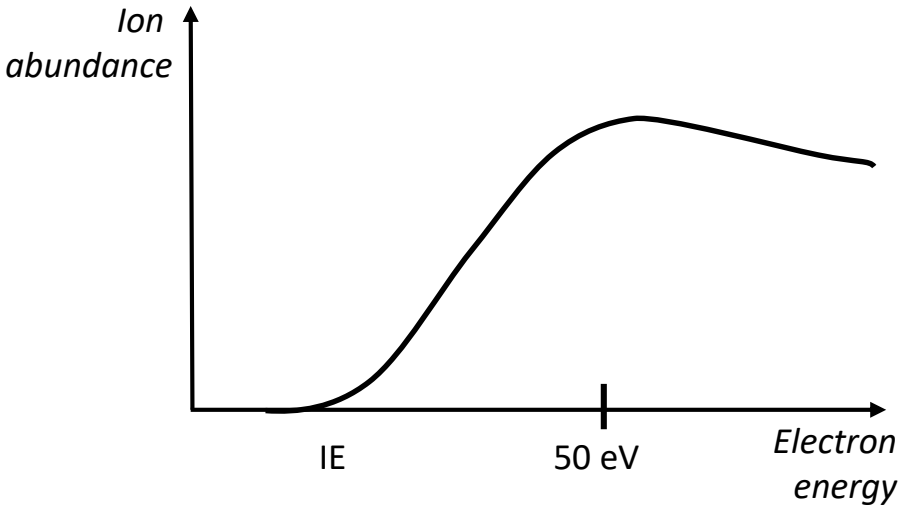

Organic molecules: IE ~ 8-12 eV for neutrals, higher for charged species.

Abundant fragmentation induced by electron ionization at 50 eV.

The neutral form is not always ionized: interaction with an electron can lead to an internal energy increase without ionization.

Electron capture dissociation

- Nowadays, Electron Capture Dissociation (ECD) applied to the charge reduction of a positive multiply charged precursor ion:

$$(\mathrm{P}, n\mathrm{H})^{n+} + e^- \rightarrow (\mathrm{P}, n\mathrm{H})^{(n-1)+\bullet *} \rightarrow \mathrm{F}_1^{i+} + \mathrm{F}_2^{(n-1-i)+\bullet}$$

- Reaction products are directly measured by mass spectrometry and ECD can be considered as the other activation methods in tandem mass spectrometry.
- Other terms and acronyms are to be used for other variations on ion / electron interactions.

Neutralisation – reionisation for sector mass spectrometers (NRMS)

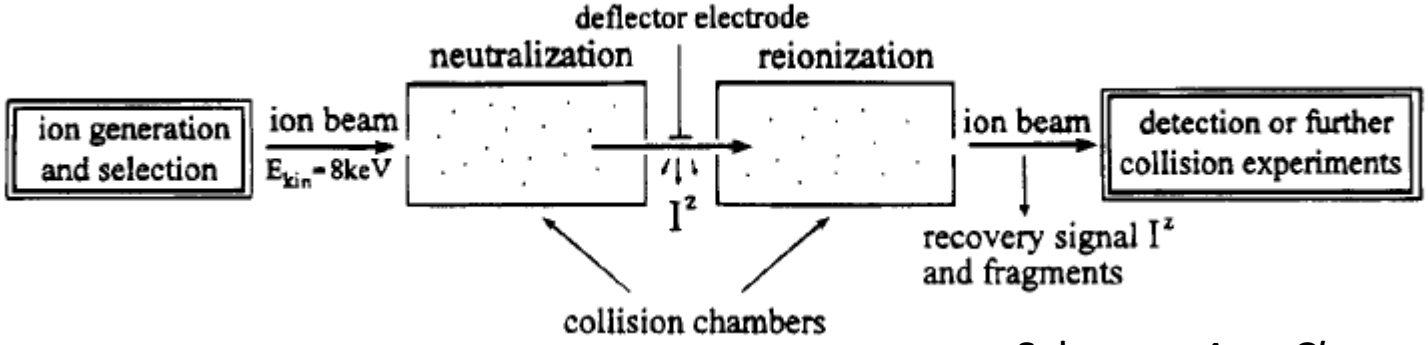

Schwarz, *Acc. Chem. Res.* 1994

- Neutralisation :
  - Various gases can be used (Xe, Hg, Na, Zn, NH_3, NO, …)
  - Electron transfer to / from the ion in the beam
- Reionisation :
  - In general O_2 leading to a positively charged product.
- The kinetic energy of the ions / molecules brings the necessary energy to achieve the endothermic reactions if necessary (usually the case for reionisation).

Electron transfer dissociation

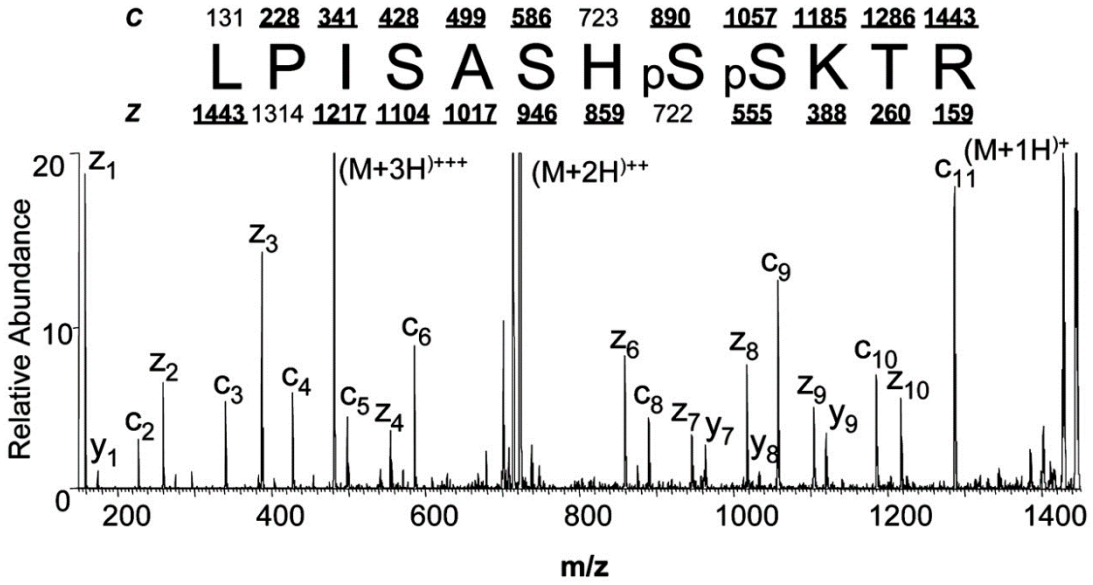

$$(M, 3H)^{3+} + A^{-} \rightarrow (M, 3H)^{2+\bullet *} + A^{\bullet} \rightarrow F_1^{+} + F_2^{+\bullet} + A^{\bullet}$$

A = $C_4H_9^-$ / $C_4H_{11}^-$ formed in a negative CI source (CH_4)

Syka et al, PNAS, 2004

EXPERIMENTAL SET UPS

Reusing the electron ionisation filament of the ion cell

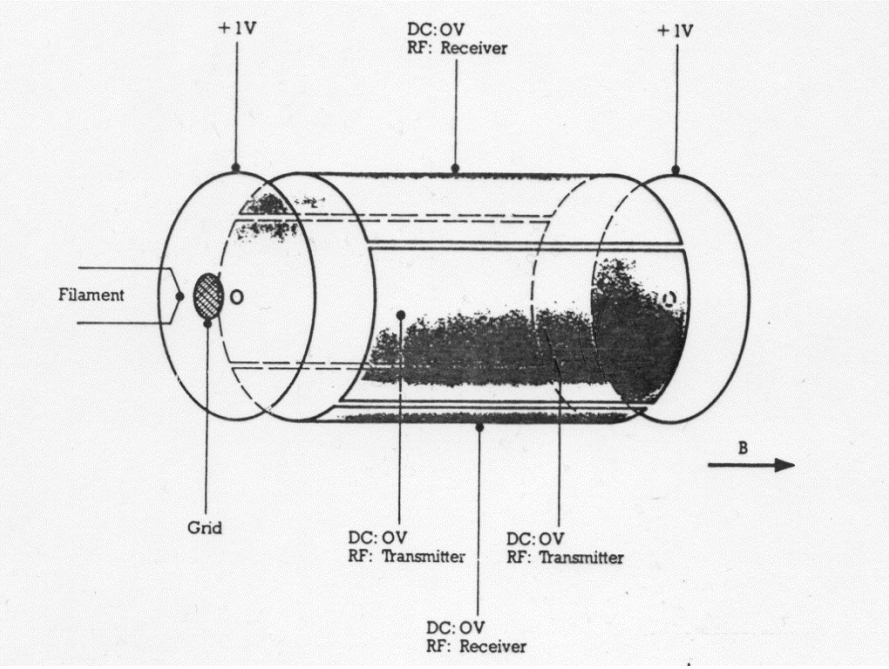

Issues:

- Low electron flux
- Low overlap of the electron beam from the filament with the ion cloud in the cell.
- Main axis of the instrument is also used by the external ion introduction / laser for activation.

Cathode and hollow cathodes

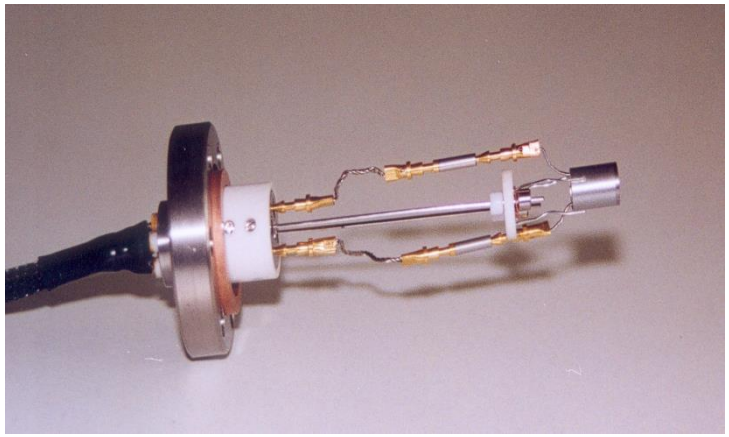

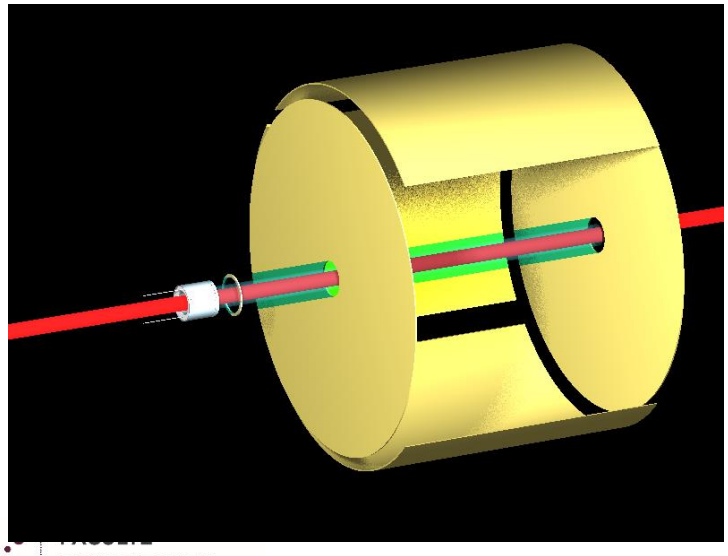

Indirectly heated cathodes have replaced the filament:

- Higher electron current
- Improved overlap of the electron beam and ion cloud.
- Additional extraction lens allows to contron electron energy independently from the electron flux.
- Hollow cathode allows combination with laser activation methods.

ECD parameters: interaction with ion trajectories

Reminder : trajectory of ions in an FT-ICR cell

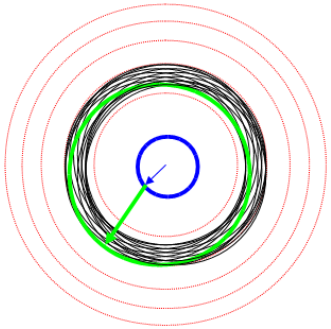

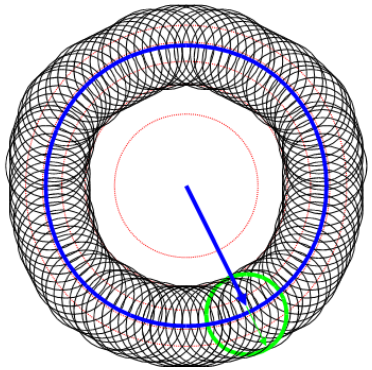

As the magnetron motion has a period on the order of kHz, for short (ms duration) irradiation, a temporal effect can be observed.
(Observed by Y. Tsybin)

$r_c + r_M < r_{outside}$

ECD in Orbitrap mass spectrometers

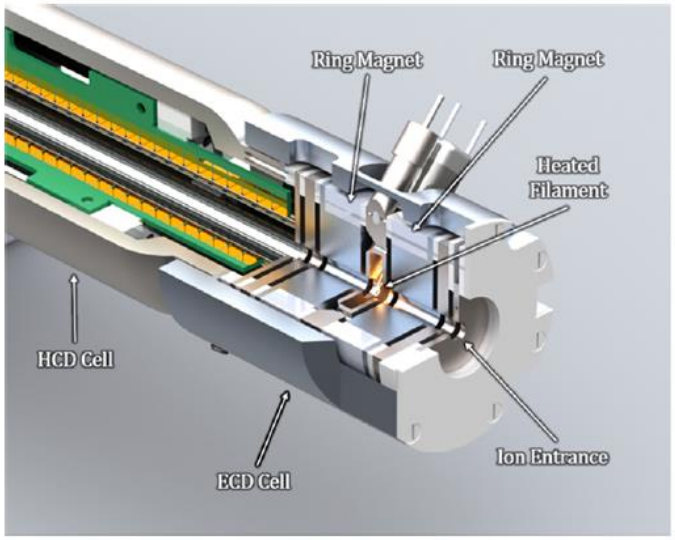

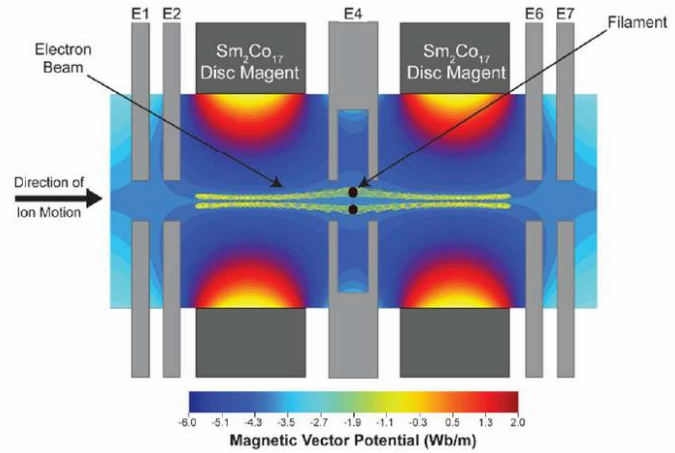

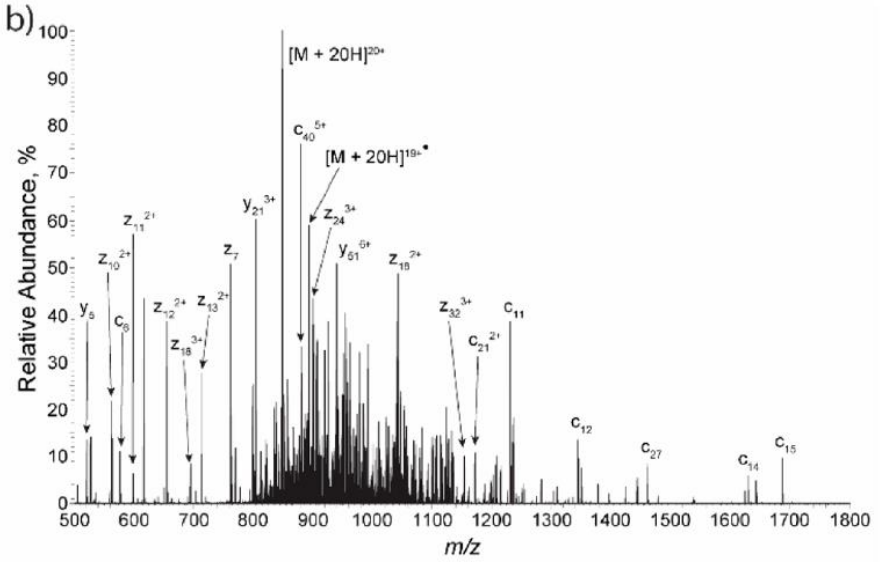

N G L S D G E W Q Q V L N V W G K V E A D I A G H G 25
26 Q E V L I R L F T G H P E T L E K F D K F K H L K 50
51 T E A E M K A S E L L K K H G T V V L T A L G G I 75
76 L K K K G H H E A E L L K P L A Q S H A T K H K I P 100
101 I K Y L E F I S D A I I H V L H S K H P G D F G A 125
126 D A Q G A M T K A L E L F R N D I A A K Y K E L G 150
151 F Q G C

K.L. Forth et al., *J. Proteome Res.* **17**, 926−933 (2018)

Instrumentation for ETD: anion sources

- « Classic » chemical ionization source

$$CH_4 + e^-_{70eV} \rightarrow CH_4^{\bullet +} + e^-_{fast} + e^-_{thermal}$$

$$A + e^-_{thermal} \rightarrow A^{\bullet -}$$

ou

$$AH + e^-_{thermal} \rightarrow A^- + H^\bullet$$

- Negative APCI source, along the same scheme with N_2 as the moderator gas.

Ion traps can confine anions and cations in the same space

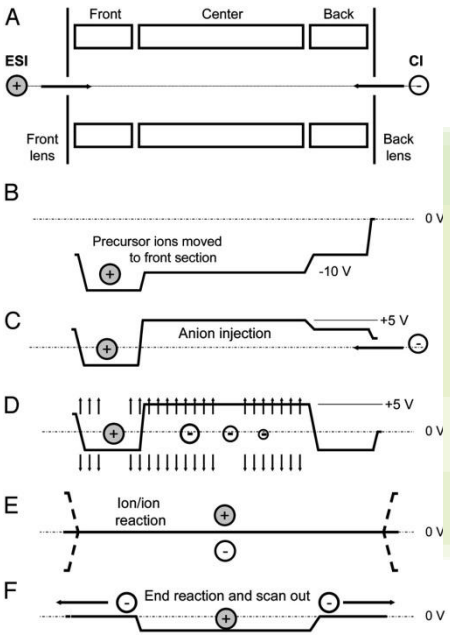

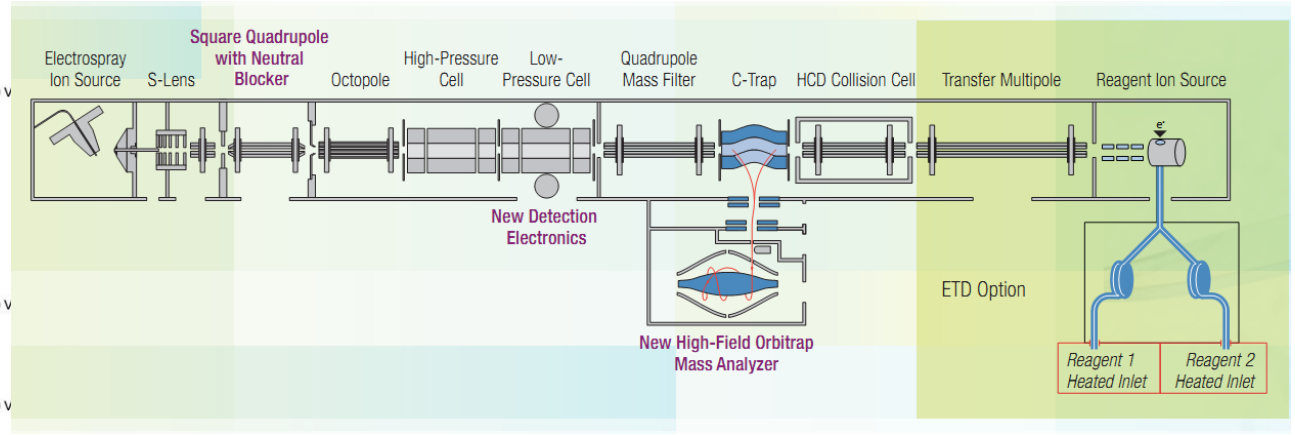

Syka et al, PNAS, 2004

Competitive reaction: Proton transfer vs electron transfer

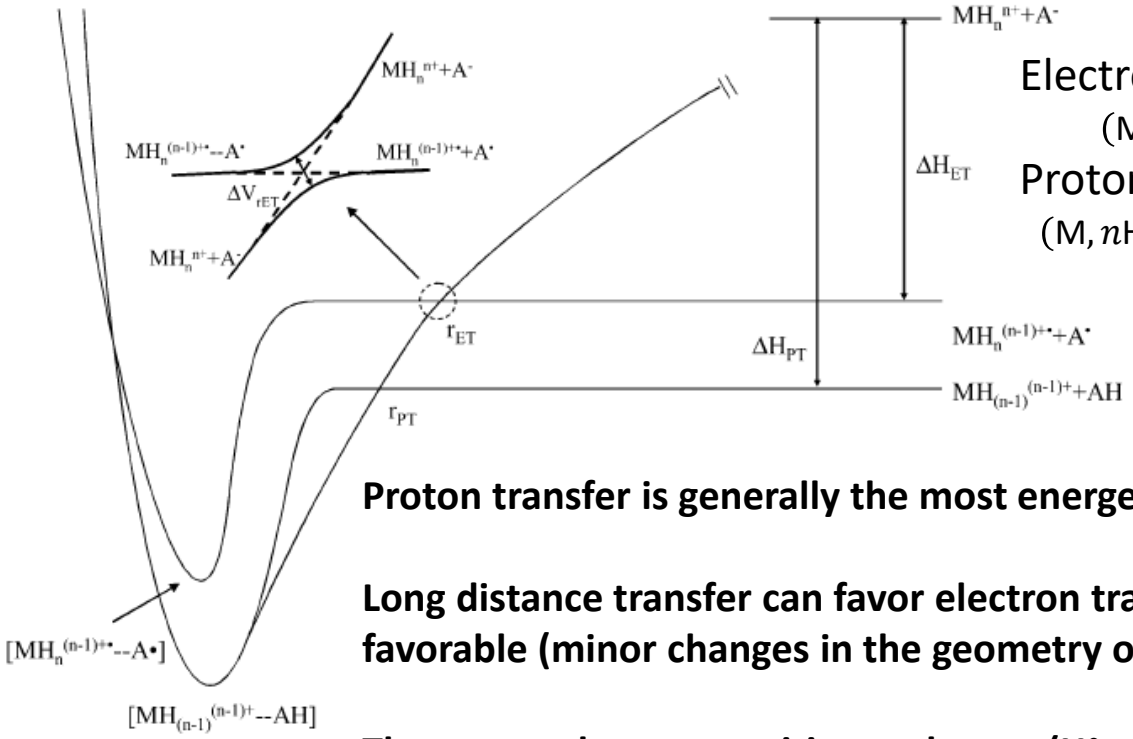

Electron transfer:

$$(\mathrm{M}, n\mathrm{H})^{n+} + \mathrm{A}^{\bullet -} \rightarrow (\mathrm{M}, n\mathrm{H})^{(n-1)\bullet +} + \mathrm{A}$$

Proton transfer:

$$(\mathrm{M}, n\mathrm{H})^{n+} + \mathrm{A}^{\bullet -} \rightarrow (\mathrm{M}, (n-1)\mathrm{H})^{(n-1)+} + \mathrm{AH}^{\bullet}$$

Proton transfer is generally the most energetically favorable pathway

Long distance transfer can favor electron transfer when the conditions are favorable (minor changes in the geometry of the reactive species).

There are other competitive pathways (H• transfer, …)

Gunavardena, *J. Am. Chem. Soc.*, 12627 (2005)

Reagents for electron transfer

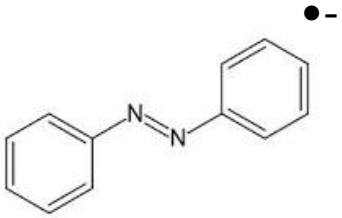

$CS_2^{\bullet-}$

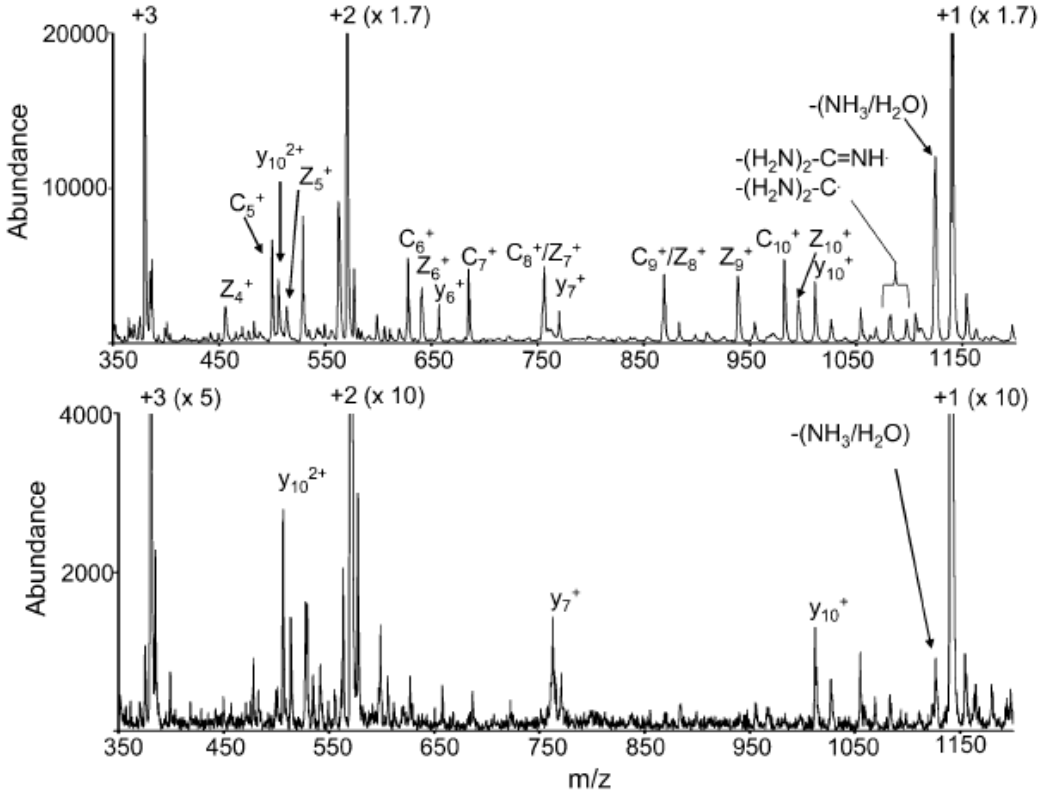

c,z major ions

y fragments

Figure 4. Post ion/ion reaction spectra of KGAILKGAILR $[M + 3H]^{3+}$ and (a) the azobenzene molecular anion and (b) $CS_2^{-\bullet}$.

Gunavardena, *J. Am. Chem. Soc.*, 12627 (2005)

28 reagents were systematically investigated

reagent	Franck–Condon factor[a] $\langle 0\|0\rangle^2$	Franck–Condon factor $\Sigma \langle 0\|\leq 10\rangle^{2}$ [b]	EA (A) (kcal/mol)	% ETD[c,d]	R^e
norbornodiene[f]	6.5×10^{-3}	1.1×10^{-2}	5.6[g]	7.2	0.10
cis-stilbene[f]	5.8×10^{-5}	5.2×10^{-3}	10.4[h]	9.8	0.60
O_2	4.9×10^{-2}	9.7×10^{-1}	10.4[g]	4.9	0.81
CS_2	2.9×10^{-8}	4.9×10^{-5}	11.8[j]	<0.01	
azobenzene	1.6×10^{-1}	1.8×10^{-1}	13.1[g]	48.8	0.86
fluoranthene	3.6×10^{-1}	3.6×10^{-1}	14.5[j]	37.4	0.96
perylene	4.1×10^{-1}	4.1×10^{-1}	22.4[g]	20.9	0.88
nitrobenzene[k]	1.3×10^{-1}	1.4×10^{-1}	23.0[j]	14.7	0.83
SF_6	6.7×10^{-11}	6.7×10^{-11}	24.2[j]	<0.01	
SO_2	7.0×10^{-2}	4.6×10^{-1}	25.5[g]	30.1	0.86
m-dinitrobenzene	2.6×10^{-2}	2.7×10^{-1}	38.3[j]	26.6	0.87
o-dinitrobenzene	8.9×10^{-6}	1.2×10^{-4}	38.3[j]	17.2	0.83
S_2O[l]	5.6×10^{-2}	3.5×10^{-1}	43.3[g]	7.3	0.82
SO_3	2.0×10^{-10}	6.9×10^{-8}	43.8[j]	<0.01	
p-dinitrobenzene	1.6×10^{-1}	1.8×10^{-1}	46.1[j]	16.4	0.88
S_3	8.2×10^{-2}	5.2×10^{-1}	48.3[g]	7.0	0.71
O_3	4.8×10^{-2}	3.8×10^{-1}	48.5[g]	4.8	0.95
$NO_2^{\bullet}$	3.6×10^{-4}	2.3×10^{-1}	52.4[g]	8.5	0.16
1,3,5-trinitrobenzene	6.1×10^{-1}	6.5×10^{-1}	60.6[j]	7.9	0.47
CO_3	6.3×10^{-1}	9.0×10^{-1}	62.0[g]	<0.01	
$I^{\bullet}$	N/A			<0.01	
$CH_3COO^{\bullet}$	3.6×10^{-3}			<0.01	
$NO_3^{\bullet}$	4.3×10^{-3}			<0.01	
$[PDCH-F]^{\bullet}$	7.5×10^{-4}			<0.01	
H_2PO_4	3.1×10^{-10}			<0.01	
$SF_5^{\bullet}$	8.0×10^{-8}			<0.01	
HSO_4	4.3×10^{-3}			<0.01	
picric acid	4.1×10^{-8}			<0.01	

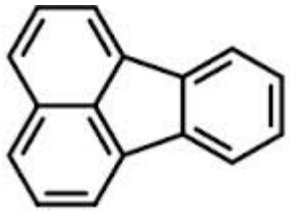

Fluoranthène

Gunavardena, *J. Am. Chem. Soc.*, 12627 (2005)

FRAGMENTATION OF PEPTIDES AND PROTEINS BY ECD AND ETD

At the molecular level

- Initial electron attachment
  - Generally suggested to be in the Rydberg orbitals.
  - Formalized by J. Simons.

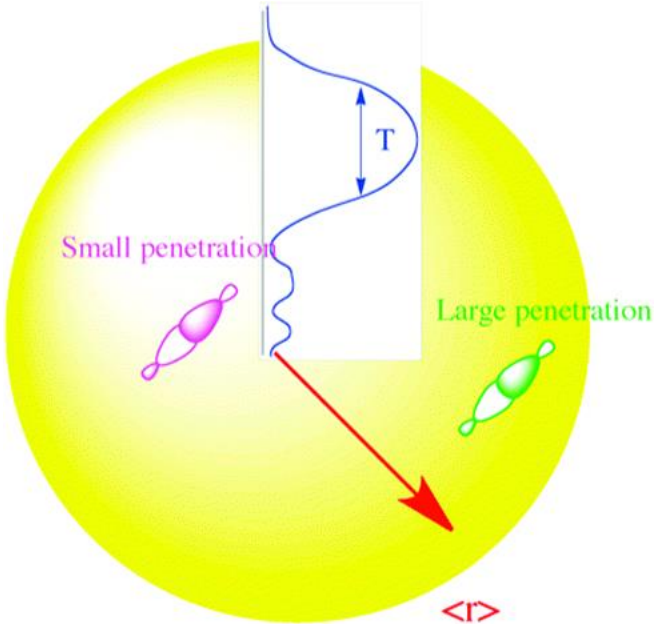

The overlap between the rydberg orbital and the lower lying orbitals towards which the electron will attach allows the electron to go towards different regions of the same polypeptide, provided that the Rydberg quantum number is sufficiently high.

J. Am. Chem. Soc. **132** 7074 (2010)

Hydrogen directed fragmentation

Electron capture at the ammonium followed by hydrogen migration; hydrogen migration can be within a hydrogen bond or change after charge reduction.

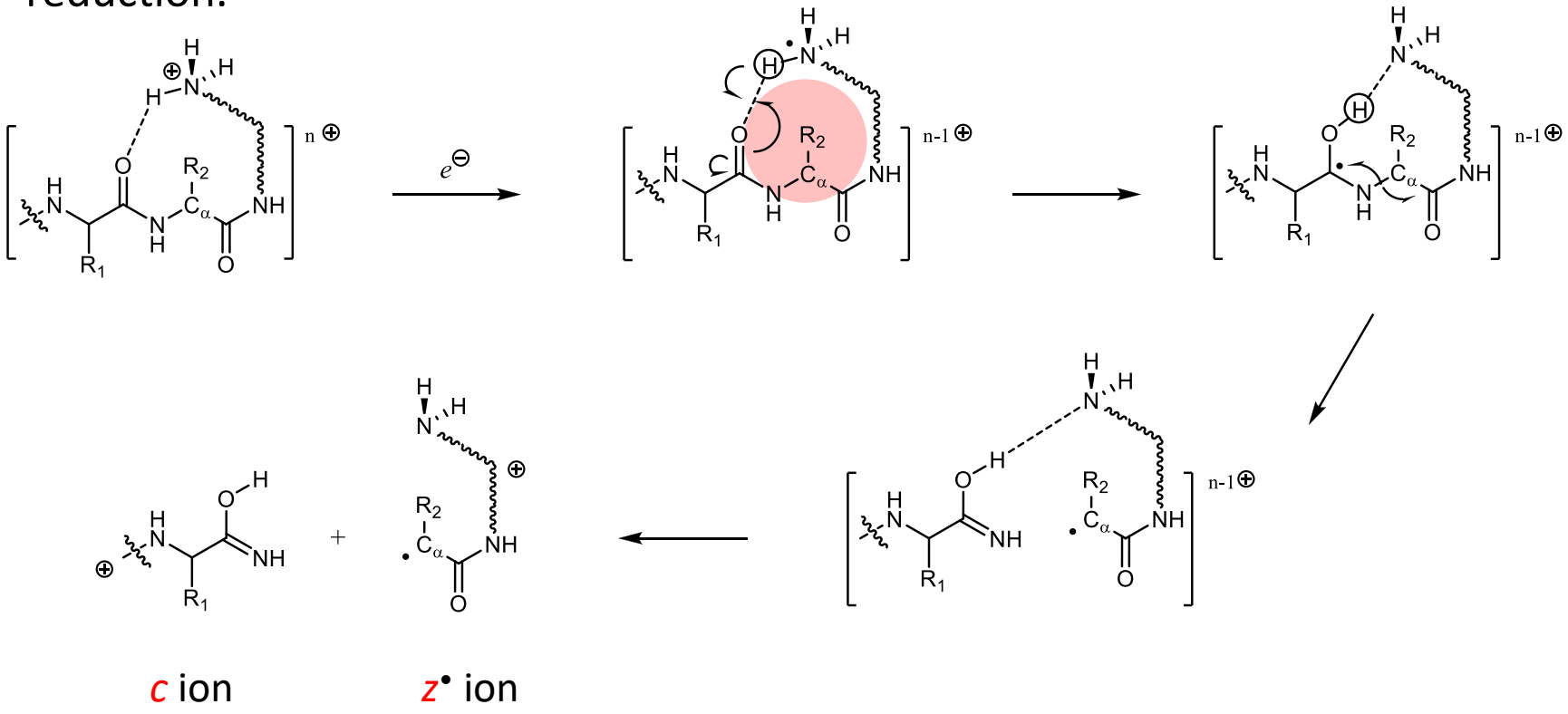

c ion *z*• ion

Zubarev , Kelleher, Mc. Lafferty *J. Am. Chem. Soc.* (1998)
Zubarev, *Eur. J. Mass Spectom.* (2002)

Carbonyl directed fragmentation (1)

Electron capture in a carbonyl π^* followed by 1. proton transfer 2. N-C_α cleavage

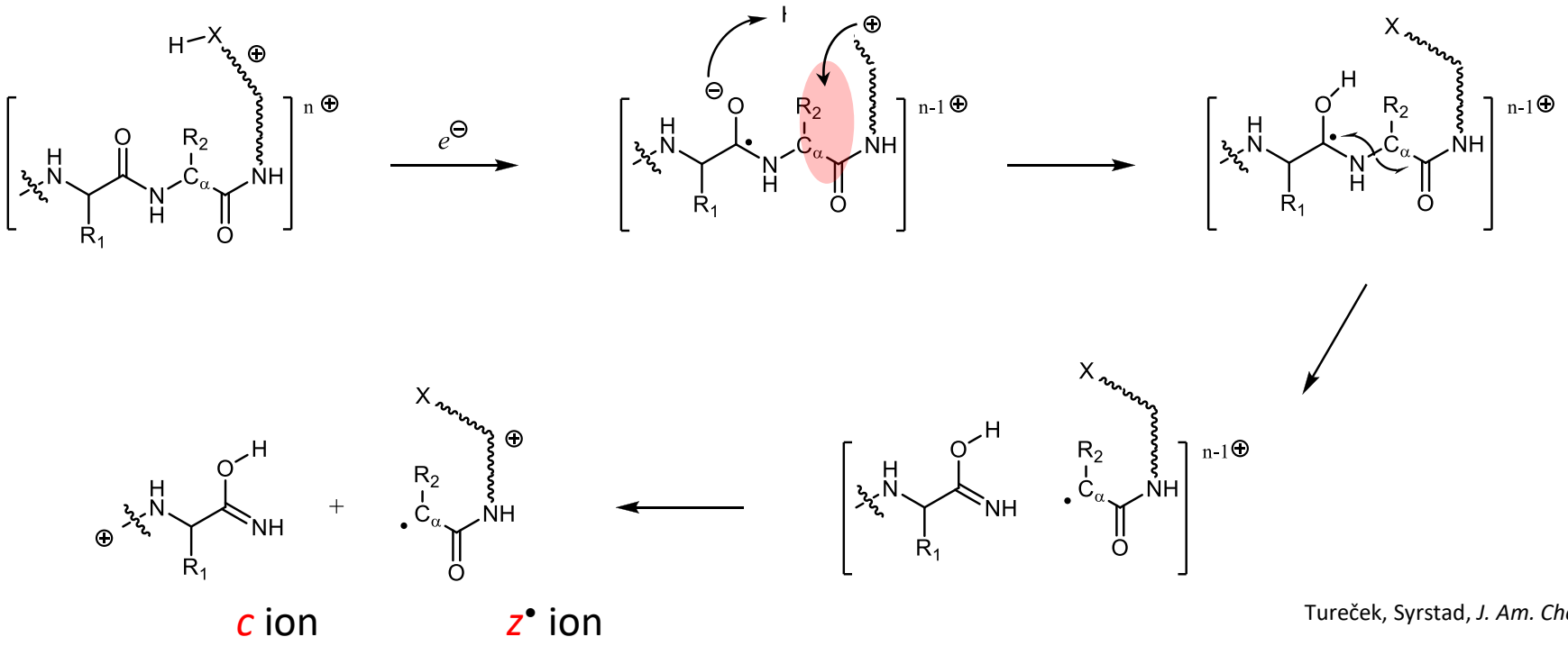

Tureček, Syrstad, *J. Am. Chem. Soc.* (2003)

Carbonyl directed fragmentation (2)

Electron capture in a carbonyl π^* followed by 1. N-C_α cleavage 2. proton transfer

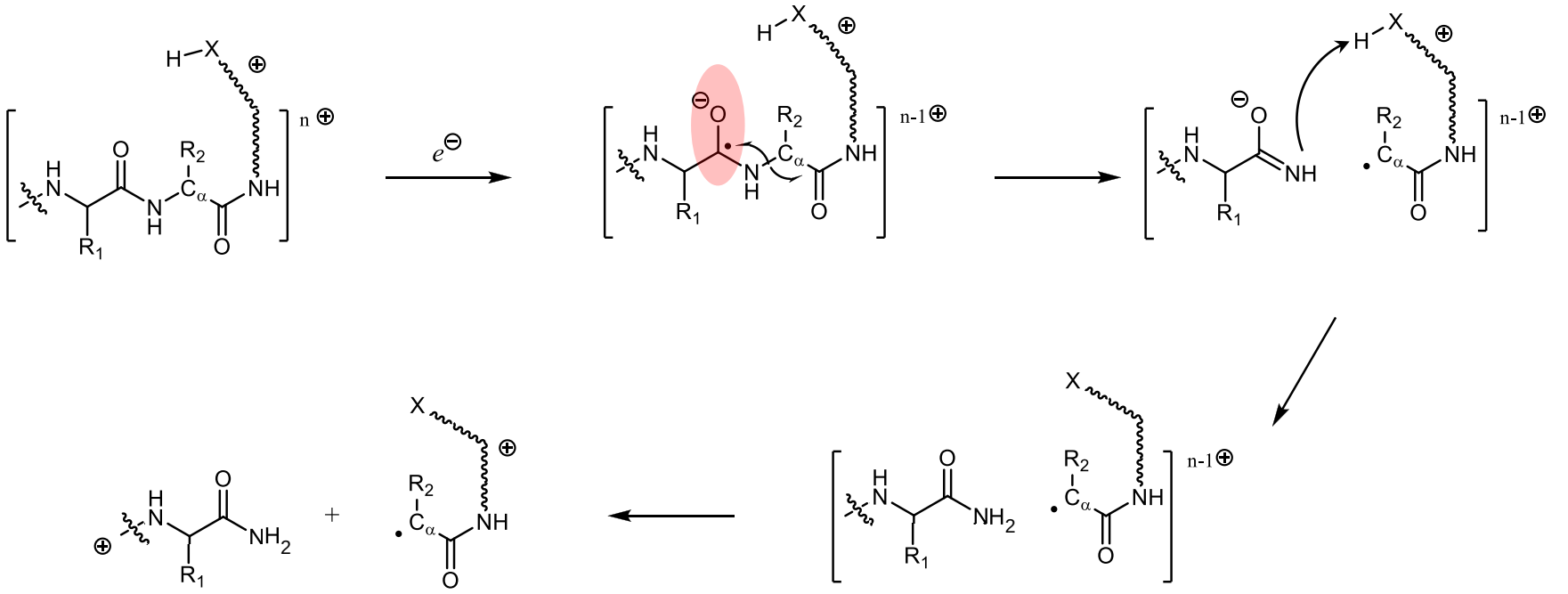

Sobczyk, M., et al., *J.Phys Chem A* (2004)

CID of a phosphorylated peptide

YEERRKSHEAV
|
OPO_3H

Mr = 1611.6
Nano-ESI, 7 µM, 4µl, SORI-CID with Xe

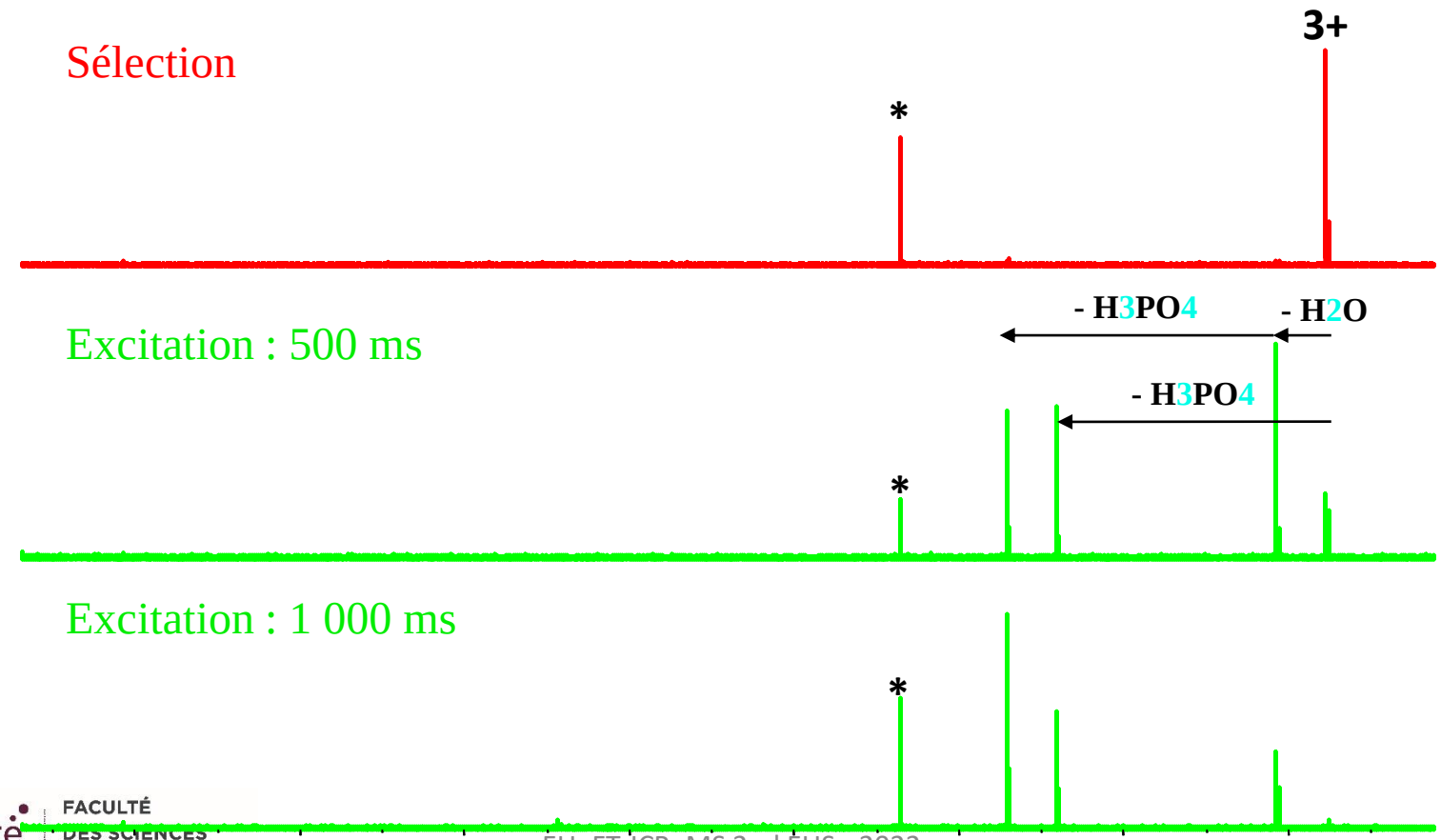

ECD of a phosphorylated peptide

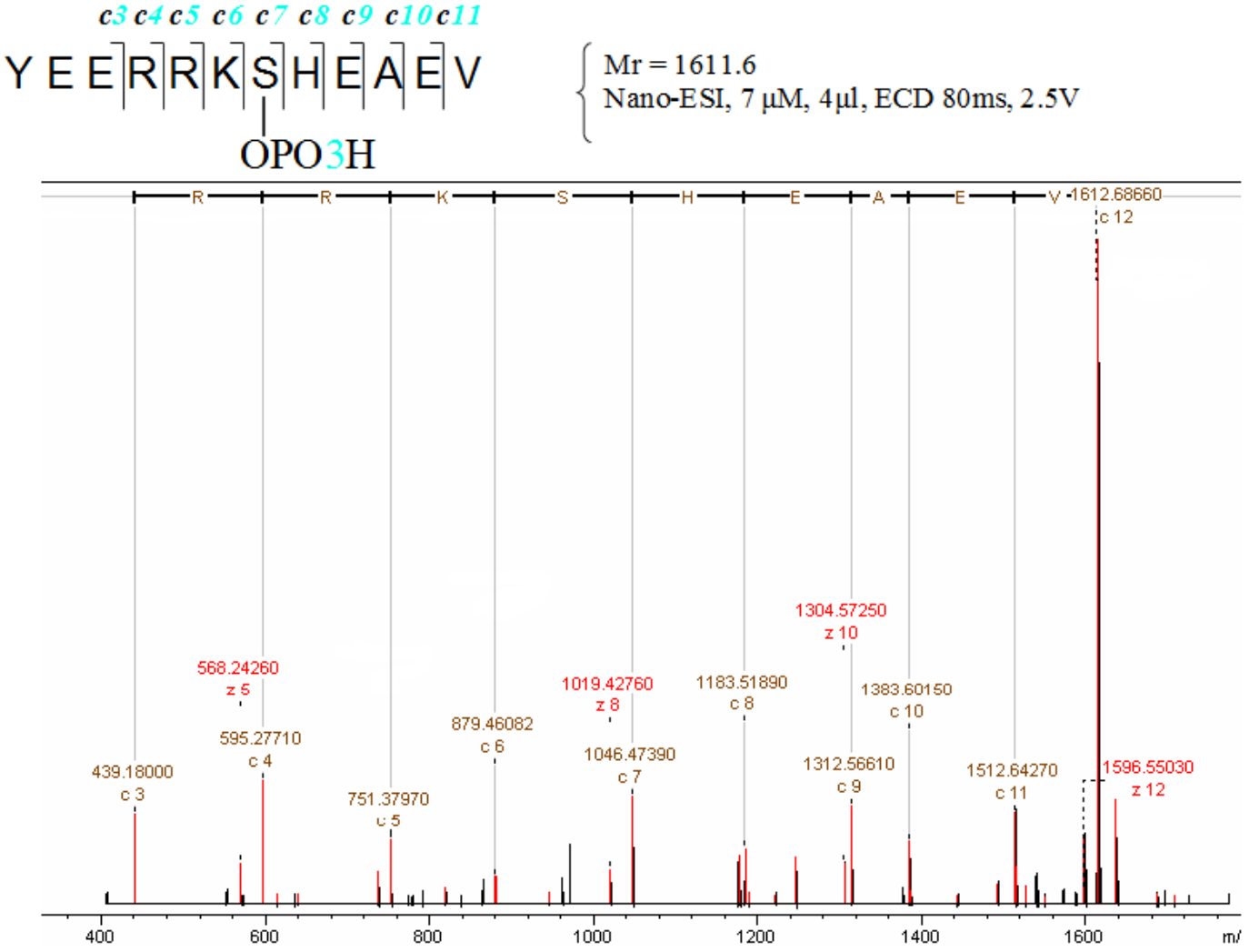

Non-covalent complexes

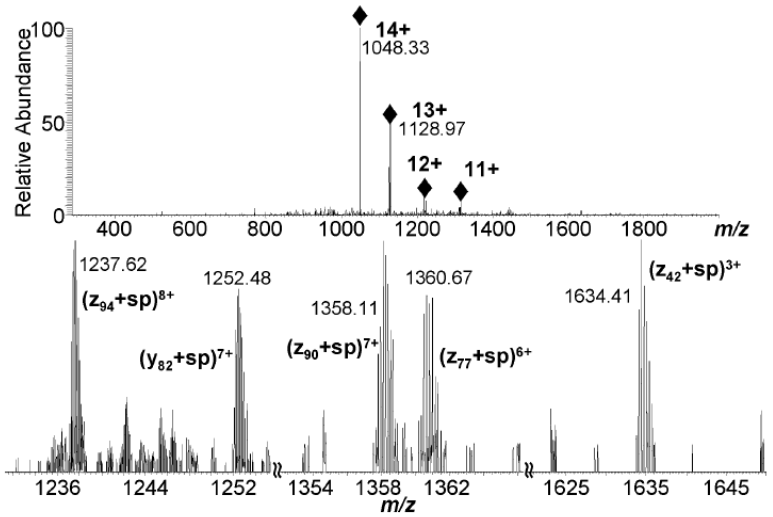

Figure 1. ECD mass spectrum of the 14+ 1:1 α-synuclein−spermine complex (*m/z* 1048; top), with expanded regions shown (bottom).

Figure 2. ECD generated products from the 14+-charged 1:1 α-synuclein−spermine complex. Product ions that retain spermine binding are indicated by the extra line underneath the fragments (e.g., L).

- Hydrogen bonds with the ligand are maintained.

Y. Xie, *J. Am. Chem. Soc.* 14432 (2006)

Locating a tannin binding site

Without 3’-OG

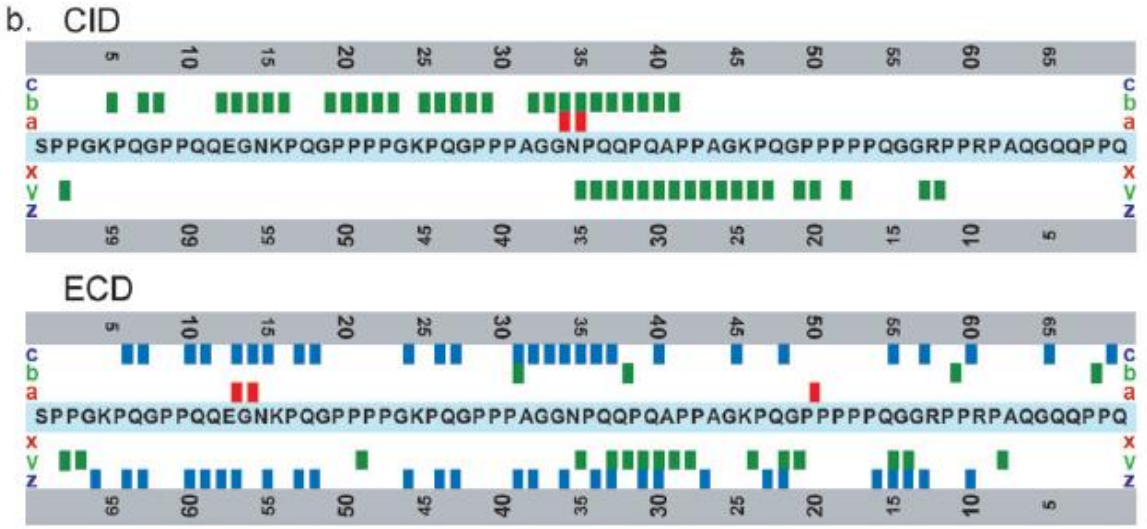

With 3’-OG

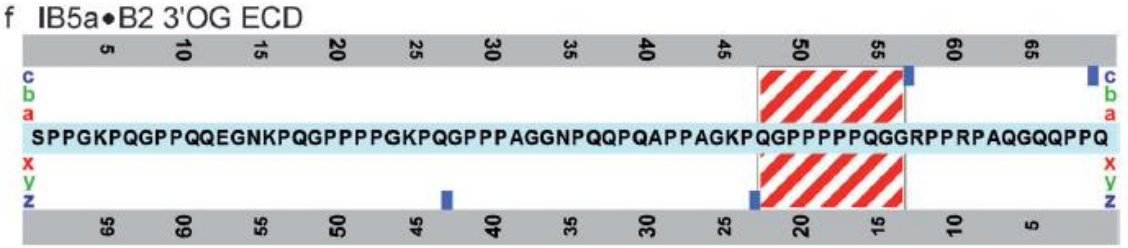

Canon, *Angew. Chem. Int. Ed.* 8377 (2013)

OTHER ELECTRON ACTIVATION MODES

The electron beam can lead to other processes

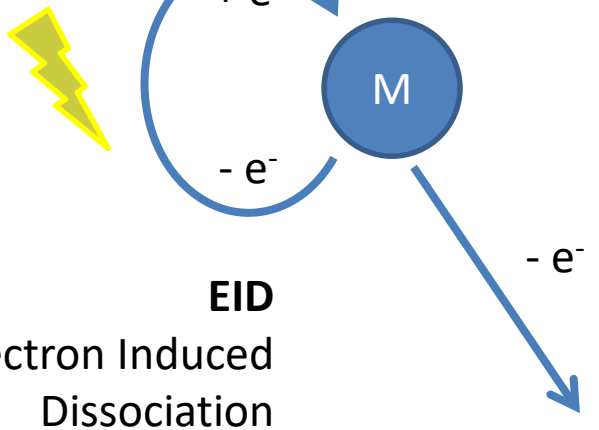

EID
Electron Induced Dissociation

Positive ions

ECD
Electron Capture Dissociation

ETD
Electron Transfer Dissociation
$A^{\bullet -}$

EI-ID
Electron Ionization Induced Dissociation

Negative Ions

ni-ECD
Negative Ion Electron Capture Dissociation

ni-ETD
Negative Ion Electron Transfer Dissociation
$A^{\bullet +}$

EDD
Electron Detachment Dissociation

EDD of oligonucleotides

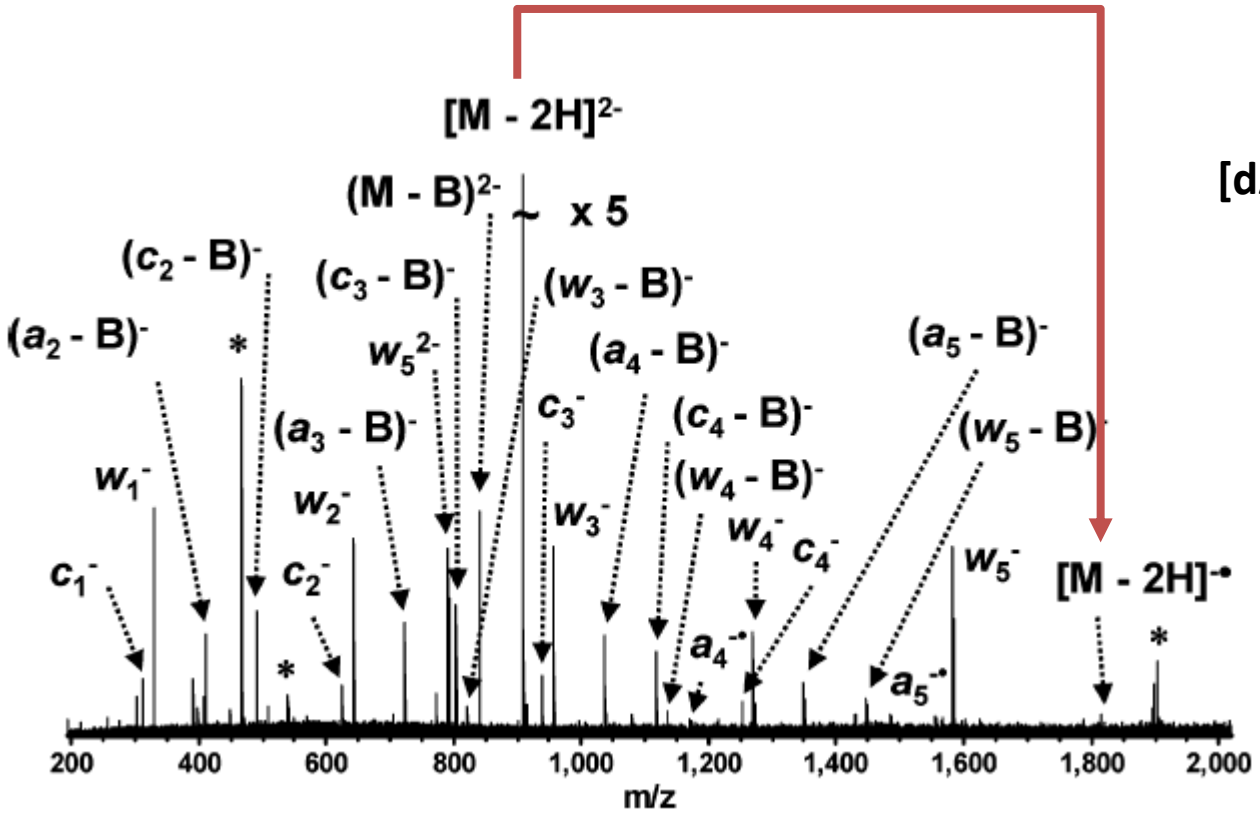

$[dA_6 - 2H]^{2-}$

1s irradiation, 17 eV

Yang, *Anal. Chem.* 1876 (2005)

Comparaison of EDD vs IRMPD on oligonucleotides

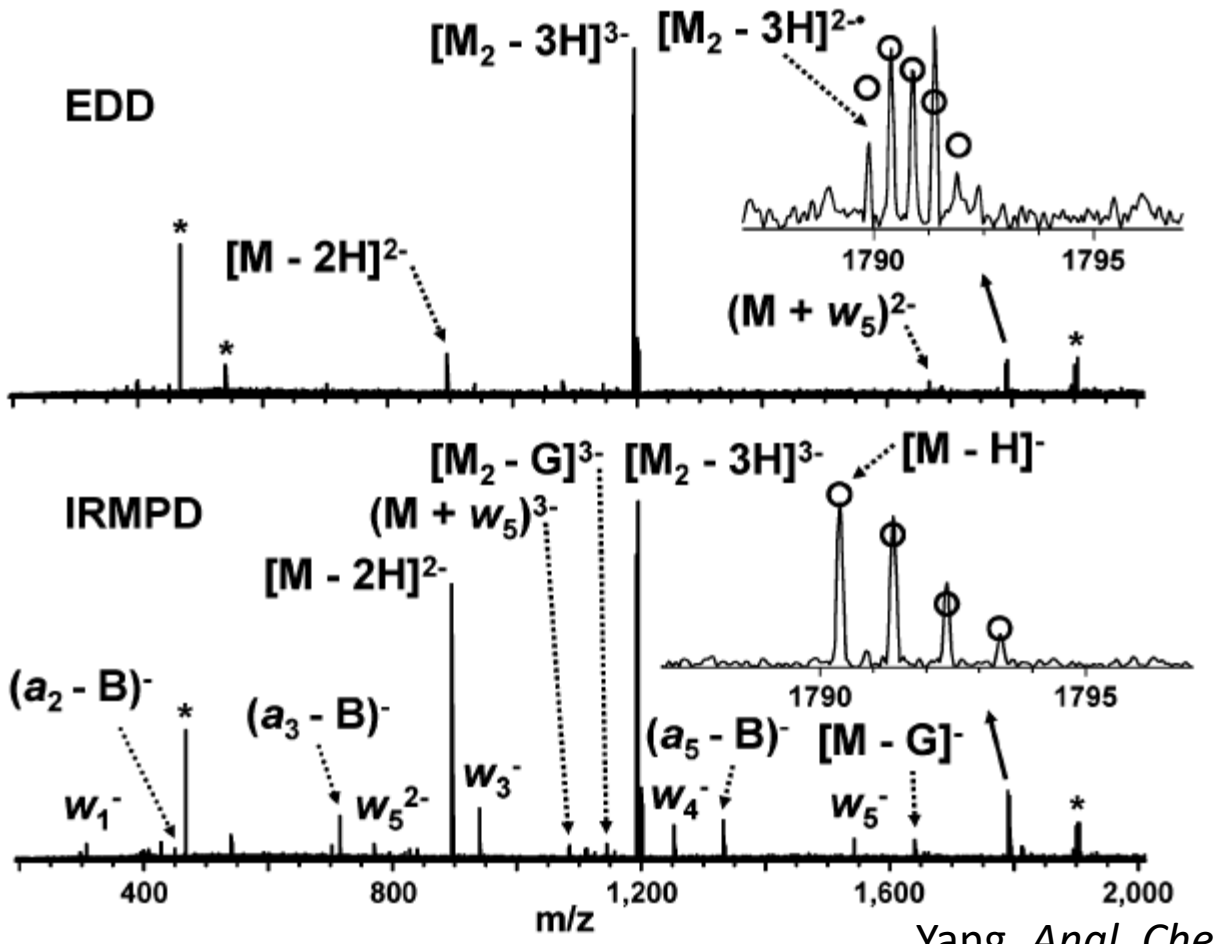

Duplex :
M = d(GCATGC)

EDD : 16 eV, 1s

IRMPD : 10 W, 150 ms

Yang, *Anal. Chem.* 1876 (2005)

Electron induced dissociation (EID)

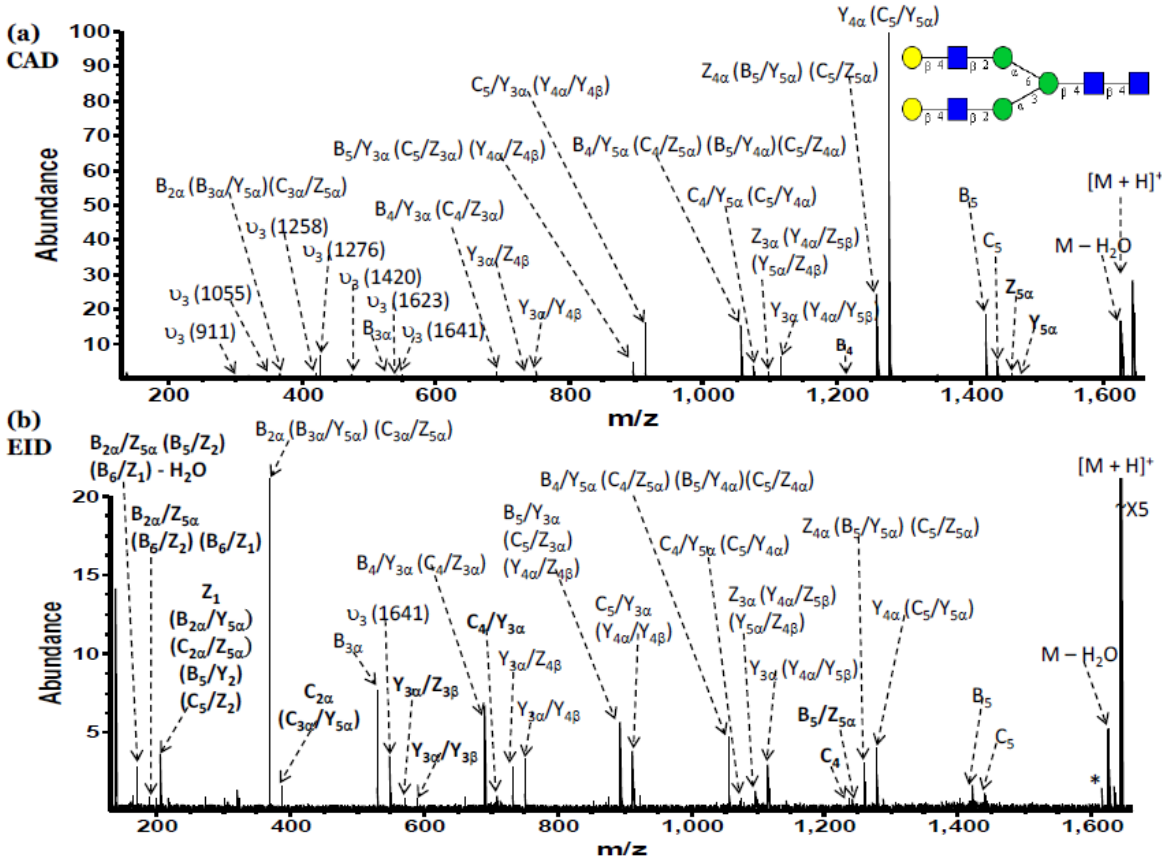

Figure 4.9 CAD and EID of an asialo, galactosylated, biantennary glycan (NA2): (a) CAD, (b) EID. For both spectra, precursor ions are labeled $[M + H]^+$. *: noise; ν_3: third harmonic peaks. Bold font indicates fragments that are unique to CAD or EID.

Bias : -11 to -20 V
Irradiation time:
0,3 – 0,5 s

Gao, PhD Thesis, Univ. Of Michigan, 2013

Acknowledgements

Philippe Maître
Debora Scuderi
Estelle Loire

infranalytics

EU FT-ICR MS

Horizon 2020
Programme

Laboratoire de Chimie Moléculaire (Palaiseau)
Gilles Frison
Gilles Ohanessian
Edith Nicol

And all of you for your attention.